A thesis presented for the degree of
Master of Science

Closed loop Control of PMSM Motor

Field Oriented Control using Hall sensors

Shawon Kumar Baral

Integrated Circuits and Systems Division
Electrical Engineering Department
Linköping University
SE-581 83 Linköping, Sweden.
November 23, 2021.

Master of Science Thesis in Electrical Engineering
Closed loop Control of PMSM Motor,
Field Oriented Control using Hall sensors
Shawon Kumar Baral
LiTH-ISY-EX–21/5444–SE

Supervisor
Tomas Uno Jonsson
ISY, Linköping University

Examiner
Lars Eriksson
ISY, Linköping University

Integrated Circuits and Systems Division
Electrical Engineering Department
Linköping University
SE-581 83 Linköping, Sweden.
November 23, 2021.

Abstract

Fossil-fuel vehicles are one of the main causes of CO2 emissions nowadays. As we are moving toward cleaner environment electrification of vehicles are becoming more and more popular. With the environment in mind, the recent improvement in battery technology and electronics has drawn a lot of attention to Brushless DC or BLDC motors. Due to their high torque output and robust design, BLDC motors are a popular choice as the main propulsion unit in electric vehicles. Permanent magnet synchronous motor, PMSM, is also a brushless dc motor with minor changes in design. So the word BLDC and PMSM is used interchangeably. In this thesis, two motor control algorithms were investigated. 6-Step control and Field oriented control or FOC. A three-phase inverter allows these motors to be driven by a battery. But when battery voltage goes down the speed of the motor also goes down. This thesis investigates a method to maintain the same speed at lower dc voltage. Also running of other motors than the control system was designed for. The control system performs well in simulation for two of the motor tested with the FOC algorithm. Simulation results show that the control system can track speed and current references with minimum error. Speed controller and current controllers control each parameter independently to control the motor. Low battery simulations provide useful data that shows how the field weakening technique makes it possible to achieve higher speed at low dc voltages.

Sammanfattning

Fossildrivna fordon är en av de främsta orsakerna till koldioxidutsläpp i dag. I och med att vi går mot en renare miljö blir elektrifieringen av fordon allt mer populär. Med miljön i åtanke har den senaste tidens förbättring av batteriteknik och elektronik dragit mycket uppmärksamhet till Brushless DC- eller BLDC-motorer som ska användas som huvudframdrivningsenhet. På grund av dess höga vridmomentutgång och robusta design så är BLDC-motorer mer populära. En permanent magnetisk synkronmotor, PMSM, är också en borstlös dc-motor med mindre förändringar i designen. Så orden BLDC och PMSM används omväxlande. I denna avhandling undersöktes två motoriska styralgoritmer. 6-stegskontroll och fältorienterad kontroll eller FOC. En trefas växelriktare gör att dessa motorer kan drivas av ett batteri. Men när batterispänningen går ner går motorns hastighet också ner. Denna avhandling undersöker en metod för att bibehålla samma hastighet vid lägre likspänning, men även drift av andra motorer än vad styrsystemet var konstruerat för. Styrsystemet fungerar bra i simulering för två av de motorer som testas med FOC-algoritmen. Simuleringsresultat visar att styrsystemet kan spåra hastighet och aktuella referenser med minimalt fel. Hastighetsregulator och aktuella styrenheter kontrollerar varje parameter individuellt för att styra motorn. Simuleringar med lågt batteri ger användbara data som visar hur fältförsvagningstekniken gör det möjligt att uppnå högre hastighet vid låg likströmsspänning.

Acknowledgements

I would like to sincerely thank my supervisor, Tomas Uno Jonsson for his help and feedback during the project.

I am also thankful to Arvind Balachandran and my friend, Anton Källström.

Finally, I would like to thank my opponent for the thesis, Vinod Diwakara.

Contents

List of Figures

List of Tables

CHAPTER 1

Introduction

The rapid growth of electric vehicles in recent years has drawn lots of attention in using Permanent magnet synchronous motors (PMSM) as the main drive motor. Being lightweight and compact compared to diesel or petrol engines it is much cheaper. PMSM has no moving part other than the rotor that makes them robust and suitable for long-term use in industrial and home applications. Right now PMSMs are used where any motor is required from HVAC, cooling fan, electric scooter, and electric bikes the list goes on [1–13].

PMSM can be controlled with or without sensor feedback from the motor. With sensors, the control system is easy to develop but costly and adds more failure points to the whole system. Sensorless control on the other hand is more robust and also more complex. In this thesis, hall sensors are used by the control system to calculate motor speed and electric angle.

There are many ways to control a PMSM, for example, 6 step control, field-oriented control, and field weakening control. Field-oriented control is the main interest for this thesis but 6 step control is also investigated as it has much easier implementation.

1.1 Problem definition

This thesis aims to investigate low battery voltage situations and cases when the motor is changed or use of another motor than the control system was originally designed for. At the end of the thesis, two questions will be answered,

1. What happens when the battery voltage goes low? and how the control system will handle low battery voltage to keep steady RPM?
2. Is it possible to run a different motor without the need for a change in the control algorithm?

1.2 Thesis outline

In chapter 2, the theory of motor and control systems is discussed. Motor mathematical models, the transformation between different models, and estimation methods are discussed in this chapter.

Chapter 3 is for the simulation result. All the method discussed in the theory chapter is simulated and presented in this chapter.

Chapter 4 is for discussion based on the simulation. Simulation results provide answers asked in the first chapter.

Chapter 5 is for the conclusion and future work-related discussion.

CHAPTER 2

Theory

2.1 Electric motor fundamentals and control systems

An electric motor is a machine that can convert electricity to mechanical energy with the presence of a magnetic field. A current conducting wire in a magnetic field can be the simplest representation of an electric motor. From figure 2.1, a conductor is placed in a magnetic field, i is the direction of the current. If the direction of the magnetic field is B, then the wire will feel an electromotive force towards F. This is also known as the left-hand rule.

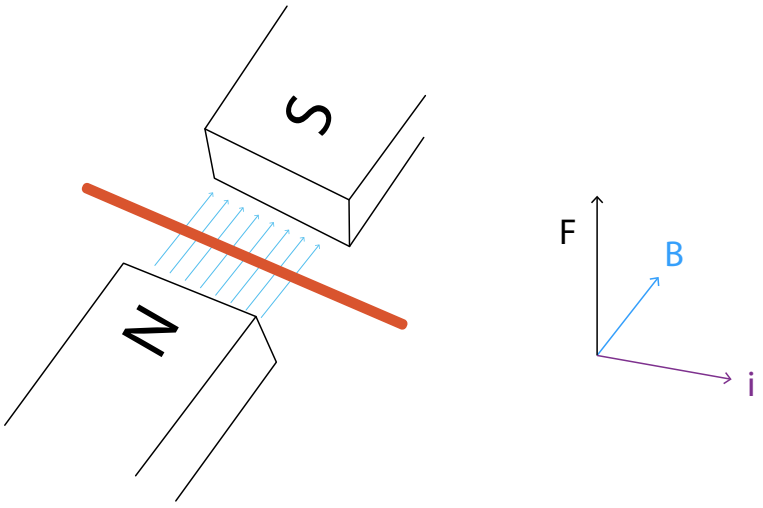

Figure 2.1: Current conducting wire in a magnetic field .

2.1.1 Brushed DC motor

The rotor, moving part of the motor, is made of an iron armature with coils. When current flows through these coils, generated magnetic fields push the magnets on the stator and this repulsion makes the rotor move. Current is delivered from the stationary housing to these moving coils through 2 pieces of metal, usually, copper is known as the brush of the motor and the motor is called Brushed dc motor. These brushes are always in contact with the rotor. There are 3 sets of coils and they are mechanically made in such a way so that the active coil can produce maximum torque. When the current coil moves current is passed through the next set of coils to produce constant torque. As the direction of current never change

these are also known as **DC motor** and this process of passing currents through different coils' is called **commutation**. DC motors' have very high starting torque this allows diverse use of these motors. But there are losses in the brush. As the brush is in contact with moving metal it wears off and requires constant maintenance. Also, the brush generates heat and spark which prohibits the use of these motors in a gas-related application.

As the rotor is moving in a magnetic field, a current is induced through the coils and generates voltage in phase with the rotor position in relation to the stator magnets. This voltage is known as Back electromotive force or simply **Back EMF**. At higher speeds, back emf can be very high and physically damage the motor and other connected components.

2.1.2 Brushless motor

To avoid the problems mentioned above, a different type of motor is used that does not have any brush, hence the name brushless DC motor. With this type of motor, the coil is stationary and the magnet is the rotor. This makes the motor robust as there is no moving electrical part. Since the coils are not moving, commutation is done electronically. Although the control system is complex, modern computers and the use of sensors makes it easier to apply these control systems.

The most commonly used brushless motors are Brushless DC (BLDC) motor and the Permanent magnet synchronous (PMSM) motor.

Both BLDC and PMSM motors are similar in configuration. They both have permanent magnets as rotors are usually made of neodymium magnets.

What makes them different is their back emf. Due to stator winding construction BLDC motor produces trapezoidal back emf and PMSM produces sinusoidal voltage shown in figure 2.2.

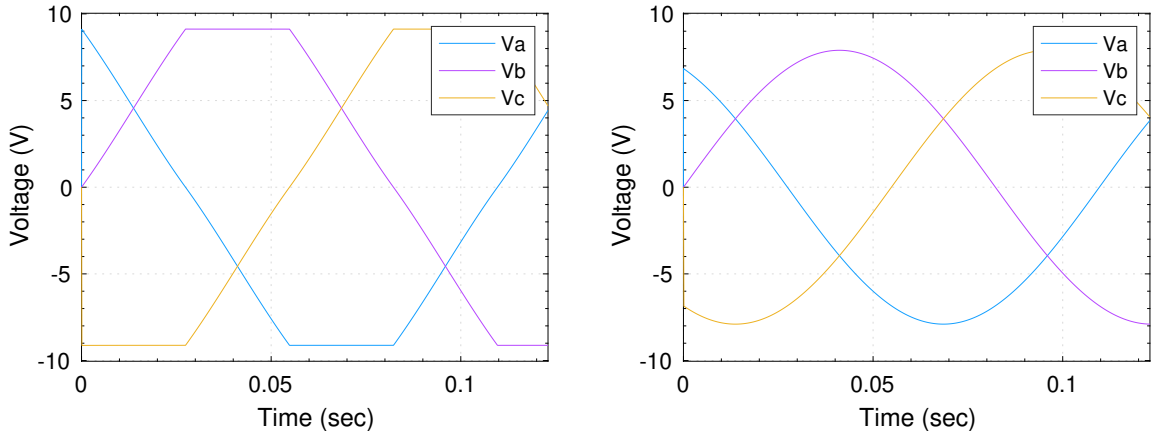

(a) BLDC.

(b) PMSM.

Figure 2.2: Back EMF

2.1.2.1 PMSM types and motor inductances

Depending on the rotor design, PMSMs can be of several types. Merrill's rotor, interior magnet, surface magnet, inset, and symmetrical buried to name a few [14]. Among all other types two most commonly used PMSMs are Interior PMSM and Surface mounted PMSM. Shown in figure 2.3. Due to the difference in magnetic path interior PMSM has different d-axis inductance and q-axis inductance [15] . In surface-mounted magnets, both paths have same inductance path, shown in figure 2.4a. So $L_d = L_q$. Figure 2.4a shows L_d and L_q inductances. Figure 2.4b shows high and low inductance paths for L_q and L_d. So for IPMSM $L_d \neq L_q$.

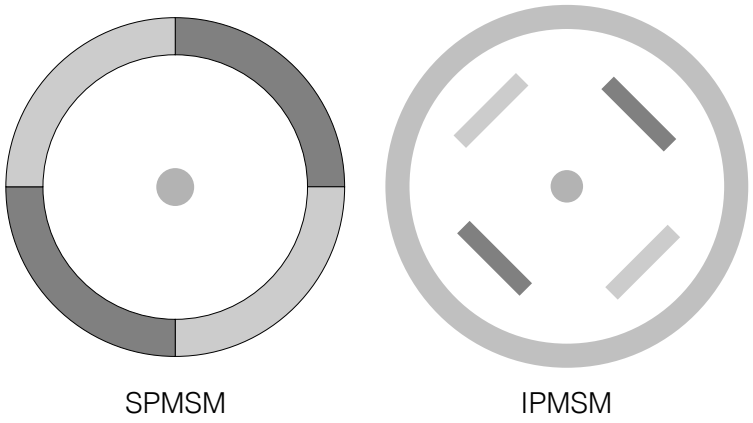

Figure 2.3: SPMSM and IPMSM.

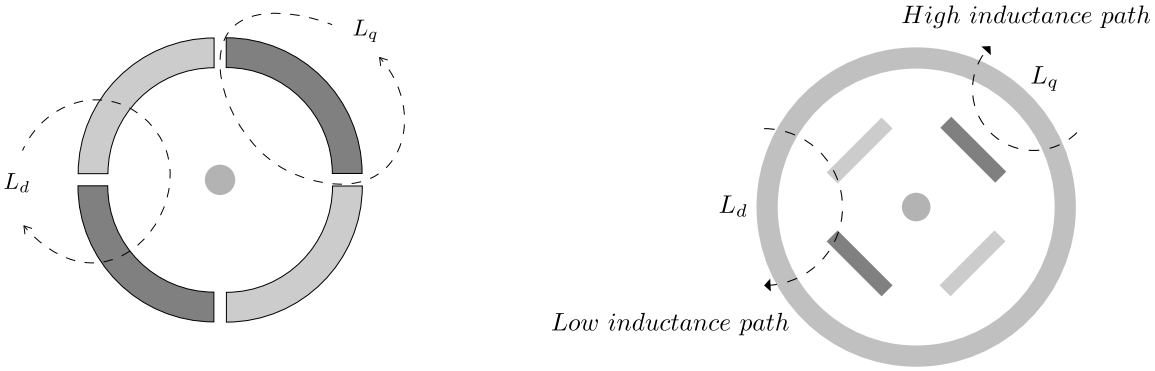

(a) Magnets on the surface of the rotor.

(b) Magnets inside the rotor.

Figure 2.4: Motor inductance path.

2.1.3 Motor pole pairs, mechanical and electrical properties

Motor stator poles usually come in pairs. This is generally referred to as either number of poles or pole pair number. In this thesis, poles are counted as pairs and written in pairs. Pole pair directly correlates to the electrical and mechanical properties of the motor. A few other important parameters are the

motor's mechanical speed, angle, and electric speed and angle.

The physical speed of the rotor is mechanical speed. and the rotor's physical angular velocity is the mechanical angle of the rotor. But electrical parameters are required by the controller to calculate and estimate different parameters and maintain the stability of the whole control algorithm.

The following equations show the relation between mechanical and electrical parameters.

$$\omega_e = pp \times \omega_m \tag{2.1}$$

$$\theta_e = pp \times \theta_m \tag{2.2}$$

Here,
ω_e = Electrical speed of the motor in Rad/s
ω_m = Mechanical speed of the motor in Rad/s
θ_e = Rotor electrical angle in Rad
θ_m = Rotor mechanical angle in Rad
pp = Motor pole pair

2.1.4 Control hardware and commutation

Usually PMSMs' have 3 coils in Y or Δ configuration. Their inductance and resistance can be represented as 3 phase balanced system shown in figure 2.10. This 3 phase system can be controlled by applying different voltages at a different node.

3 phase inverter is used to connect motor terminals to either high or low DC voltage shown in figure 2.5. To run the motor different gate pulse is used from a high-speed microcontroller to turn on or off each MOSFET. Speed of the motor is controlled by using pulse-width modulated(PWM) gate pulse. PWM techniques are discussed in later sections of this thesis.

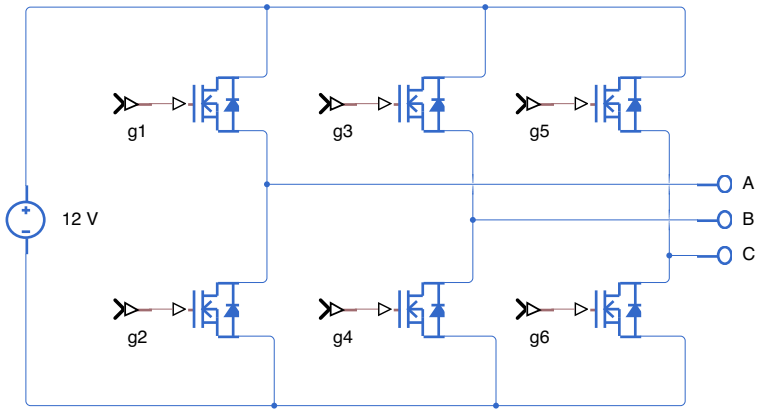

Figure 2.5: 3 phase h-bridge configuration.

2.1.5 Rotor position sensor

To apply correct voltage at the different nodes the control system needs position feedback from the motor. One of the cheapest ways is using hall sensors. In one motor there are 3 sensors placed 120 degrees apart from each other, shown in figure 2.6. These are digital hall sensors. They change their output from $0 \rightarrow 1$ or $1 \rightarrow 0$ when the magnetic pole of the rotor changes.

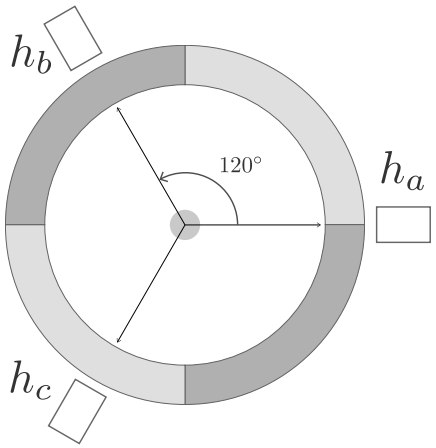

Figure 2.6: Hall sensor position.

2.2 6 Step control

The easiest and cheapest way to run a PMSM is to apply DC voltage at each node based on hall sensors output [16]. In table 2.1 shows which voltage to be applied based on the hall sensor combination. Here +1 denotes full DC voltage and -1 is ground and 0 means no connection. Based on this combination it is possible to get the gate signals required to apply the correct voltage at each node. These combinations are shown in table 2.2. This table is used by the microcontroller to turn on/off MOSFETs. From table 2.2 it is clear that only 6 steps are needed to move the rotor. This is why it is called a **6-Step control system**. These steps are repeated sequentially by the microcontroller to run the motor. The order of the steps determines the direction of the motor. So changing the order from $1 \rightarrow 6$ to $6 \rightarrow 1$ will change the motor's direction.

Hall			emf		
a	b	c	a	b	c
0	0	0	0	0	0
0	0	1	0	-1	+1
0	1	0	-1	+1	0
0	1	1	-1	0	+1
1	0	0	+1	0	-1
1	0	1	+1	-1	0
1	1	0	0	+1	-1
1	1	1	0	0	0

Table 2.1: Hall signals to emf conversion.

	emf			Gate signals					
Step	a	b	c	g1	g2	g3	g4	g5	g6
1	0	-1	+1	0	0	0	1	1	0
2	-1	+1	0	0	1	1	0	0	0
3	-1	0	+1	0	1	0	0	1	0
4	+1	0	-1	1	0	0	0	0	1
5	+1	-1	0	1	0	0	1	0	0
6	0	+1	-1	0	0	1	0	0	1

Table 2.2: emf to gate signal conversion.

2.2.1 Problem with 6 step control

The table 2.1 shows that the motor coils are energized between high and low voltages. This high voltage switching creates torque ripple. This is unwanted as ripple can cause vibration, unwanted noise, and unsmooth operation. Another problem is only 2 phases are active at a time, which reduces possible output power. To avoid these problems sinusoidal voltage is applied to the gates of the inverter so that the motor runs smoothly without any torque ripple.

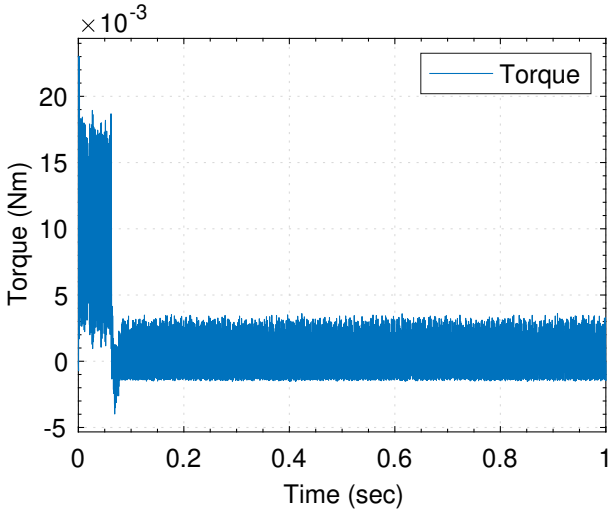

Figure 2.7: Torque ripple in 6 step control.

Through field-oriented control, it is possible to apply sinusoidal voltage at the motor. To control the motor with a microcontroller, a simplified mathematical model is required which is discussed in the next section.

2.3 Field oriented control

The basic principle of field-oriented control is to run the motor with sinusoidal voltage to achieve smooth torque while producing maximum torque. Maximum torque is generated, when the angle between the stator's magnetic field and the rotor's magnetic field is 90 degrees. This control system continuously makes an adjustment to align the stator magnetic field right-angled to the rotor magnetic field, hence the name **Field oriented control, FOC**. All the hardware is designed to achieve this goal.

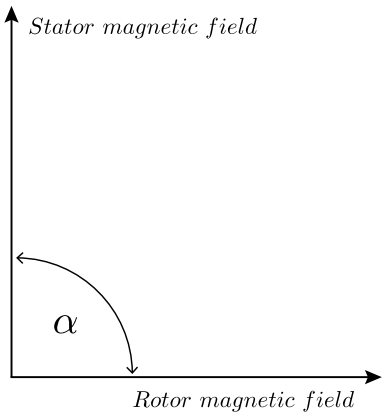

Figure 2.8: Rotor and stator magnetic field orientation for maximum torque generation.

Stator magnetic field can be represented by its vector components. One component is aligned to the rotor magnetic field called the direct axis,d, and the other one is perpendicular to the rotor magnetic field called quadrature axis,q which is shown in figure 2.9. Stator magnetic field can be aligned perpendicular to rotor magnetic field by setting d axis to 0 and adjusting q axis.

The Control system is designed to turn on or off specific MOSFET of the inverter in figure 2.5 so that necessary voltage is applied to the motor to keep correct stator magnetic field orientation. The Control system needs feedback from the motor to know if it is running properly eg. correct speed and protection from overvoltage or over current and also to detect stall.

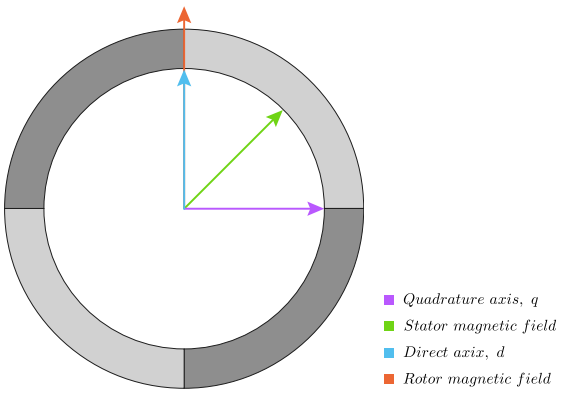

Figure 2.9: Stator magnetic field alignment.

2.3.1 Mathematical model of PMSM

A mathematical model of the motor is a requirement to apply the FOC algorithm in a digital processor so that it can predict the voltage required to keep the q axis aligned perpendicular to the d axis based on current speed and phase current measurement. The General 3 phase mathematical model is quite complex to implement in a digital processor. The following sections provide the motor's equation and a simplified model to be implemented in a microcontroller.

2.3.1.1 Motor model in *abc* frame

From the stator's point of view a motor is simply a 3 phase balanced system, shown in figure 2.10. As this is from stator's reference point this is a stationary reference frame.
Voltages at each phase is given by the following equation, [17]

$$\begin{bmatrix} v_a \\ v_b \\ v_c \end{bmatrix} = R_s \begin{bmatrix} i_a \\ i_b \\ i_c \end{bmatrix} + \frac{d}{dt} \begin{bmatrix} \Psi_{sa} \\ \Psi_{sb} \\ \Psi_{sc} \end{bmatrix} \tag{2.3}$$

Were,
v_{abc} = Phase voltages
R_s = Stator coil resistance
i_{abc} = Phase currents
Ψ_{sabc} = Stator flux
and, Ψ_{sabc} is given by [18]

$$\begin{bmatrix} \Psi_{sa} \\ \Psi_{sb} \\ \Psi_{sc} \end{bmatrix} = L_{ss} \begin{bmatrix} i_a \\ i_b \\ i_c \end{bmatrix} + \begin{bmatrix} \Psi_{ra} \\ \Psi_{rb} \\ \Psi_{rc} \end{bmatrix} \tag{2.4}$$

Were,

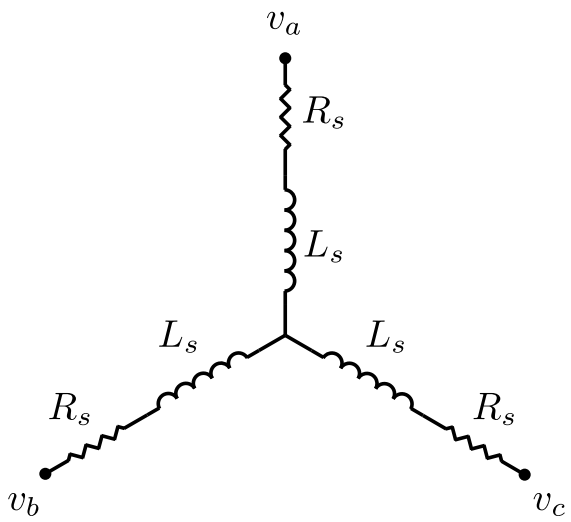

Figure 2.10: 3-phase equivalent model of PMSM.

L_{ss} = Inductance matrix, depends on motor
Ψ_{rabc} = Amplitude of the flux generated by the permanent magnets

$$\begin{bmatrix} \Psi_{ra} \\ \Psi_{rb} \\ \Psi_{rc} \end{bmatrix} = \Psi_r \begin{bmatrix} \cos(\theta_e) \\ \cos(\theta_e - 2\pi/3) \\ \cos(\theta_e + 2\pi/3) \end{bmatrix} \tag{2.5}$$

Here,
θ_e = Electrical angle of the rotor
Ψ_r = Amplitude of the flux generated by the permanent magnets

So the equation 2.3 can be written as,

$$\begin{bmatrix} v_a \\ v_b \\ v_c \end{bmatrix} = R_s \begin{bmatrix} i_a \\ i_b \\ i_c \end{bmatrix} + \frac{d}{dt} L_{ss} \begin{bmatrix} i_a \\ i_b \\ i_c \end{bmatrix} + \Psi_r \frac{d}{d\theta_e} \begin{bmatrix} \cos(\theta_e) \\ \cos(\theta_e - 2\pi/3) \\ \cos(\theta_e + 2\pi/3) \end{bmatrix} \tag{2.6}$$

2.3.1.2 *abc* to $\alpha\beta$ transformation (Clarke Transformation)

A three-phase system is a balanced three-phase system if the signals are in the following form [19]

$$x_a = A\cos(\omega t + \varphi) \tag{2.7}$$
$$x_b = A\cos(\omega t + \varphi - 2\pi/3) \tag{2.8}$$
$$x_c = A\cos(\omega t + \varphi + 2\pi/3) \tag{2.9}$$

For balanced system,

$$x_a + x_b + x_c = 0 \tag{2.10}$$

These variables may be voltage, current or magnetic flux. This three-phase system can be simplified to 2 phases by applying **Clarke Transformation** named after the inventor Edith Clarke [20].

$$\begin{bmatrix} x_\alpha \\ x_\beta \end{bmatrix} = \sqrt{\frac{2}{3}} \begin{bmatrix} 1 & -\frac{1}{2} & -\frac{1}{2} \\ 0 & \frac{\sqrt{3}}{2} & -\frac{\sqrt{3}}{2} \end{bmatrix} \begin{bmatrix} x_a \\ x_b \\ x_c \end{bmatrix} \tag{2.11}$$

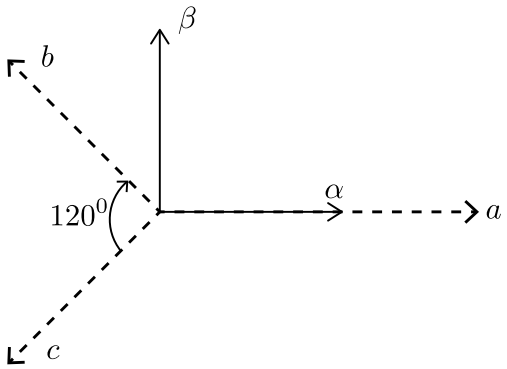

Figure 2.11: *abc* to $\alpha\beta$ transformation.

2.3.1.3 Motor model in $\alpha\beta$ frame

Motor model in $\alpha\beta$ frame can be found by applying above transformation to the equation 2.6 [21].

$$\frac{d}{dt}\begin{bmatrix} i_\alpha \\ i_\beta \end{bmatrix} = -\frac{R_s}{L_s} + \frac{1}{L_s}\left(\begin{bmatrix} v_\alpha \\ v_\beta \end{bmatrix} - \begin{bmatrix} e_\alpha \\ e_\beta \end{bmatrix}\right) \tag{2.12}$$

Were,
$i_{\alpha\beta}$ = Stator currents
$v_{\alpha\beta}$ = applied stator voltages
L_s = Stator inductance
$e_{\alpha\beta}$ = Back EMF

and $e_{\alpha\beta}$ is given by [18],

$$e_\alpha = -\sqrt{\frac{3}{2}}\Psi_r\ \omega_e \sin\theta_e \tag{2.13}$$

$$e_\beta = \sqrt{\frac{3}{2}}\Psi_r\ \omega_e \cos\theta_e \tag{2.14}$$

Here,
Ψ_r = Amplitude of the flux generated by the permanent magnets
ω_e = Electrical speed of the rotor
θ_e = Electrical angle of the rotor

2.3.1.4 $\alpha\beta$ to dq transformation (Park Transformation)

Although $\alpha\beta$ frame is reduced to 2 phases this reference frame is stationary. This is 2 phase projection of the 3 phase model from the stator's point of view. Also, the differential terms in equation 2.12 can be hard and inefficient to compute by a microprocessor. To make them simpler these equations need to be transformed to get the rotor's perspective which will be in the rotation. This transformation is also known as **Park Transformation**.
Which is given by,

$$\begin{bmatrix} x_d \\ x_q \end{bmatrix} = \begin{bmatrix} \cos\omega t & \sin\omega t \\ -\sin\omega t & \cos\omega t \end{bmatrix}\begin{bmatrix} x_\alpha \\ x_\beta \end{bmatrix} \tag{2.15}$$

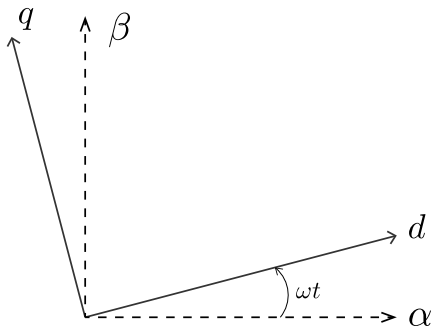

Figure 2.12: $\alpha\beta$ to dq transformation.

2.3.1.5 Motor model in dq frame

Motor model in dq frame is obtained by applying Park transformation [22] on equation 2.12. Which is,

$$\frac{di_d}{dt} = \frac{v_d}{L_d} - \frac{R_s\ i_d}{L_d} + \frac{L_q}{L_d}.\omega_e.i_q \tag{2.16}$$

$$v_d = R_s i_d + L_d \frac{di_d}{dt} - \omega_e.L_q.i_q \tag{2.17}$$

and,

$$\frac{di_q}{dt} = \frac{v_q}{L_q} - \frac{R_s.i_q}{L_q} - \frac{L_d}{L_q}.\omega_e.i_d - \lambda\frac{\omega_e}{L_q} \tag{2.18}$$

$$v_q = R_s i_q + L_q \frac{di_q}{dt} + \omega_e.L_d.i_d + \lambda\omega_e \tag{2.19}$$

Here,
$i_{d,q}$ = d-axis and q-axis currents
$v_{d,q}$ = d-axis and q-axis voltages
$L_{d,q}$ = d-axis and q-axis inductance
R_s = Coil resistance
ω_e = Electrical speed of the rotor
λ = Permanent magnet flux linkage.

2.3.1.6 Electromagnetic torque

Torque in dq frame is given by,

$$T_e = \frac{3}{2}pp[\lambda i_q + (L_d - L_q)i_d i_q] \tag{2.20}$$

Rotor speed w_r is given by,

$$J\frac{d}{dt}\omega_r = T_e - f_v\omega_r - T_l \tag{2.21}$$

For the motor used in this thesis equation 2.21 becomes,

$$J\frac{d}{dt}\omega_r = pp * i_q\left[\frac{3}{2}pp[\lambda i_q + (L_d - L_q)i_d i_q]\right] - f_v\omega_r - T_l \tag{2.22}$$

Here,
i_q = Current in q axis
i_d = Current in d axis
L_q = q Axis inductance

$L_d =$ d Axis inductance
$pp =$ Number of pole pairs
$J =$ Inertia moment
$f_v =$ Viscous friction coefficient
$T_l =$ Load torque

2.3.2 Field Oriented Control implementation

FOC control algorithm constantly solves equations 2.17 and 2.19 to keep rotor and stator magnetic fields aligned as mentioned in section 2.3. Differential terms in those equations can be ignored for the steady-state as there is no change in currents in the steady-state.

Starting from the current measurement, phase currents are measured from the motor terminal, shown in figure 2.13. Then Clarke and Park transformation is applied to generate i_d and i_q currents. Which is then compared with the reference, to generate the error. The error signal is then amplified by the PI controllers. The decoupling block simultaneously calculates v_{dd} and v_{qd} to control d-axis and q-axis voltage independently of their d and q axis currents. These voltages are added with the PI controllers' output to generate v_d and v_q voltages. Inverse Carke transform then followed by Inverse Park transform generates abc voltages that are required by PWM generator to generate Space vector modulated signals. Which is then fed to the inverter that generates 3 phase voltage for the motor.

In summery FOC algorithm performs the following steps sequentially.

1. Measure motor speed and phase currents
2. Transform phase currents into 2 phase system, $abc \rightarrow \alpha\beta$, using Clarke transformation
3. Perform $\alpha\beta \rightarrow dq$ using Park transformation
4. Calculate v_{dd} and v_{qd} independently using i_d and i_q from Park transformation.
5. Calculate Output v_d and v_q from measured phase currents and decoupling block.
6. Apply inverse Park transformation, $dq \rightarrow \alpha\beta$ and inverse Clarke transformation, $\alpha\beta \rightarrow abc$.
7. Generate space vector modulated waves from abc voltages.

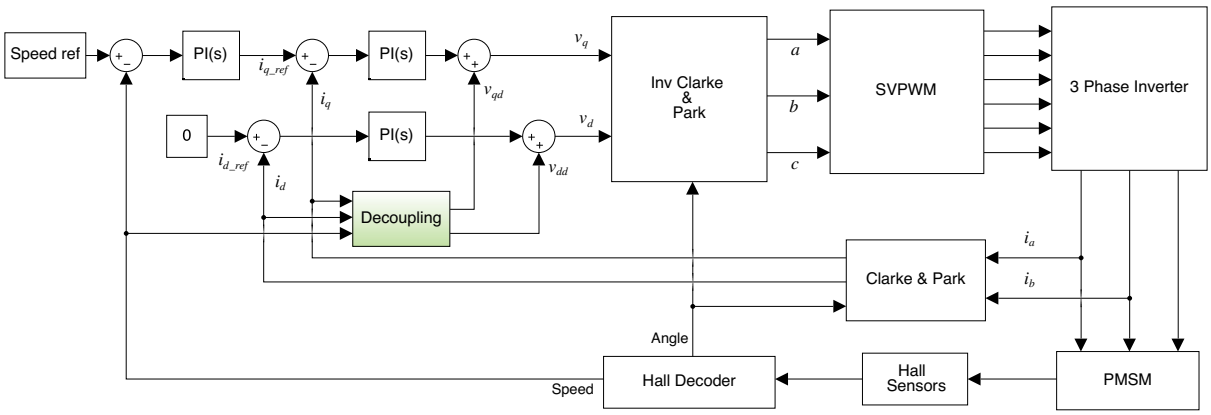

Figure 2.13: FOC algorithm.

2.3.3 Stator voltage decoupling

Both d and q axis voltages must be controlled independently to have proper field-oriented control [23]. But equations 2.17 and 2.19 show that v_d is dependent on i_q and v_q is dependent on i_d. To control them independently separate equations are computed by the decouple block in figure 2.13.

The decoupling block solves the following equations to generate v_{dd} and v_{qd}.

$$v_{dd} = R_s i_d - \omega_e . L_q . i_q \tag{2.23}$$

$$v_{qd} = R_s i_q + \omega_e . L_d . i_d + \lambda \omega_e \tag{2.24}$$

2.3.4 Speed and angle feedback from motor

Information of current speed is required by the FOC algorithm to generate correct v_d and v_q voltages, also to determine if the motor is running at the speed desired speed set by the user. There are lots of ways to measure the speed of the motor. But in this thesis, speed will be calculated by hall sensors output. This method only uses software calculation, so no extra hardware is necessary.

2.3.4.1 Speed calculation from Hall sensor

Each hall sensor changes it's output whenever rotor magnet changes from $N \rightarrow S$ or $S \rightarrow N$ with 50% duty cycle.
Speed of the rotor can be calculated by the following equation [24].

$$N_s = 60 \times \frac{f}{pp} \tag{2.25}$$

Here, N_s is the rotor speed in RPM, f is the frequency of the hall sensor and pp is the number of pole pair of motor. As the duty cycle is 50%, only measurement of high time, Th is enough. Which is shown in figure 2.14.

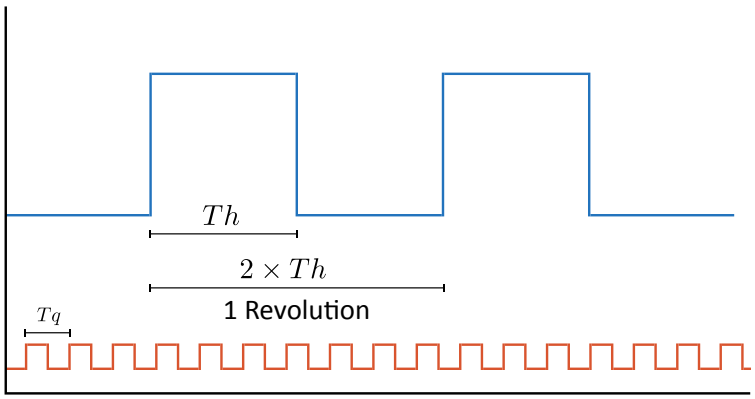

Figure 2.14: Hall sensor and interrupt generator.

To measure the high time of the hall sensor an interrupt generator is used that produces a tick with known time interval, T_q. Then, when the hall signal transitions from $0 \rightarrow 1$, a counter is incremented with each tick, T_q. When the next falling edge of hall signal is detected the counter value is stored and reset for the next cycle, which is shown in figure 2.15. Multiplying the counter value with tick interval, T_q will give hall sensor high time,T_h.

The following algorithm simplifies the frequency measurement process,

Step 1: Initiate the interrupt generator
Step 2: On the rising edge of hall sensor start the counter
Step 3: On the next falling edge stop the counter
Step 4: Store counter value and reset the counter
Step 5: Calculate f from equation 2.28
Step 6: Calculate and store rotor speed from equation 2.25
Step 7: Go to step 2.

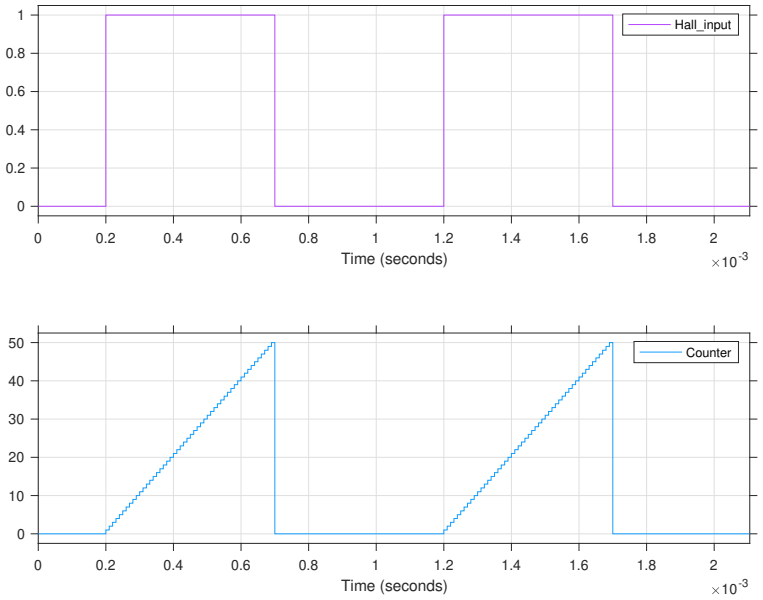

Figure 2.15: Hall sensor's frequency estimator.

From the following equations, f can be calculated. For this project, $T_q = 10\ \mu S$.

$$T_h = T_q \times N_c \tag{2.26}$$

$$T = 2 \times T_h \tag{2.27}$$

$$f = \frac{1}{T} \tag{2.28}$$

Estimating speed from one hall sensor means speed is updated at every hall change or 180°. Which can be a problem during startup or when the motor is ran at a slower speed. To avoid this problem all of the hall sensors are used. With the same algorithm mentioned above except the counter is reset at every hall change from all sensors. So reset pulse is generated from simple **edge detection** for all sensors and counter is reset at every pulse from the edge detector. In this way the algorithm gives 6 times better resolution for speed update.

2.3.4.2 Angle estimation

The angle of the motor can be easily calculated by the current speed of the motor. Equation 2.25 provides the motor's current speed in Rad/s. Simple integration over time produces an angle for the provided speed. So, angular velocity of the rotor from equation 2.28 is,

$$\omega_e = 2 \times \pi \times f \tag{2.29}$$

And rotor electrical angle,

$$\theta_e = \int \omega_e \, dt \tag{2.30}$$

Here, ω_e is electrical speed of the rotor in Rad/s, and θ_e is the electrical angle of the rotor in Radians.

As the angle keeps increasing, it needs to be reset to align with phase A back emf. This is done through correct edge of hall pulses. So the integrator is reset with correct hall edge to start the calculation again.

2.3.5 PWM techniques

2.3.5.1 Sinusoidal PWM

Pulse width modulation or PWM is a modulation technique where the width of a pulse signal or duty cycle is modulated. This modulated pulse is applied to a switch like MOSFET or IGBT to control output

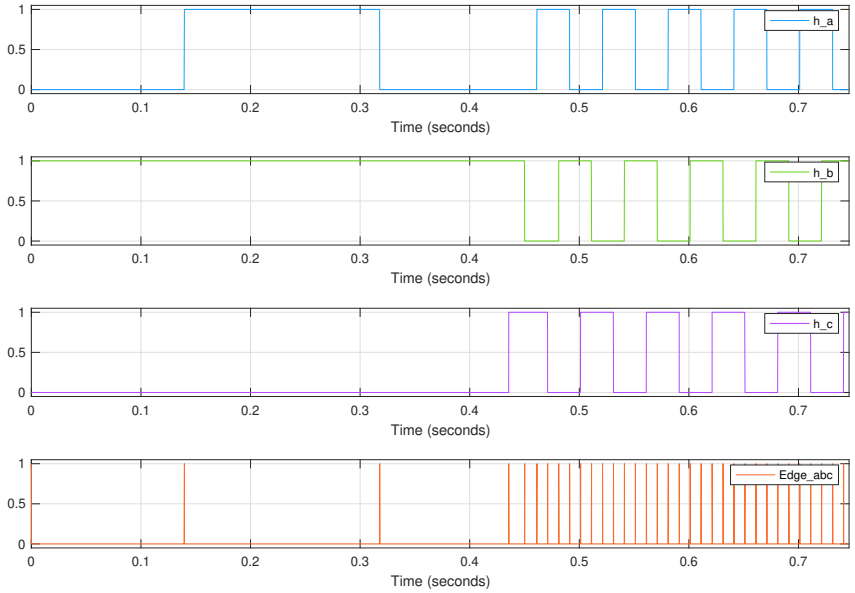

Figure 2.16: Edge detection for hall sensors.

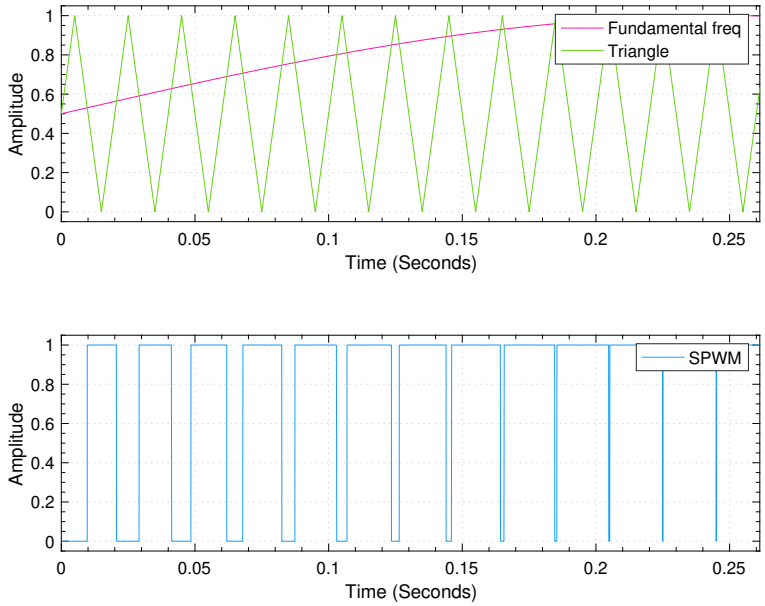

Figure 2.17: PWM generation.

voltage from a DC source. For example, speed control of a motor by changing battery voltage.
The modulator produces output 1 or 0 by comparing the amplitudes of a reference signal to a high-frequency triangular wave. If reference amplitude is greater than carrier then output is high else output is low. Figure 2.17 shows the comparison and PWM signal generation.

This 'high' time is also called the **duty cycle** and expressed in percentage. As it shows the percentage of DC voltage seen by the load. Dividing duty cycle by 100 gives modulation index. Which is another representation of the ratio between applied DC voltage to the load and total DC voltage. so for modulation index m_a, $0 \leq m_a \leq 1$. In case of $m_a > 1$, it is called over modulation.

For example, if a DC source is 24V and duty cycle is 30% or $m_a = 0.3$ that is the switch stays 30% of

the time on and 70% of the off then the voltage seen by a load will be,

$$= 24 \times \frac{30}{100}$$
$$= 7.2\ V$$

Similarly for 90% duty cycle, $m_a = 0.9$, and output voltage is,

$$= 24 \times \frac{90}{100}$$
$$= 21.6\ V$$

If a sinusoidal voltage is used as the reference then modulated PWM signal changes according to the frequency of the sinusoidal voltage shown in figure 2.19. Using a low pass filter sinusoidal voltage can be reproduced from the PWM signal. As the motor coils are huge inductors they act as low pass filters. This way AC voltage is applied from a DC source. This is why this modulator is also called an inverter and for 3 phase system, it is called 3 phase inverter.

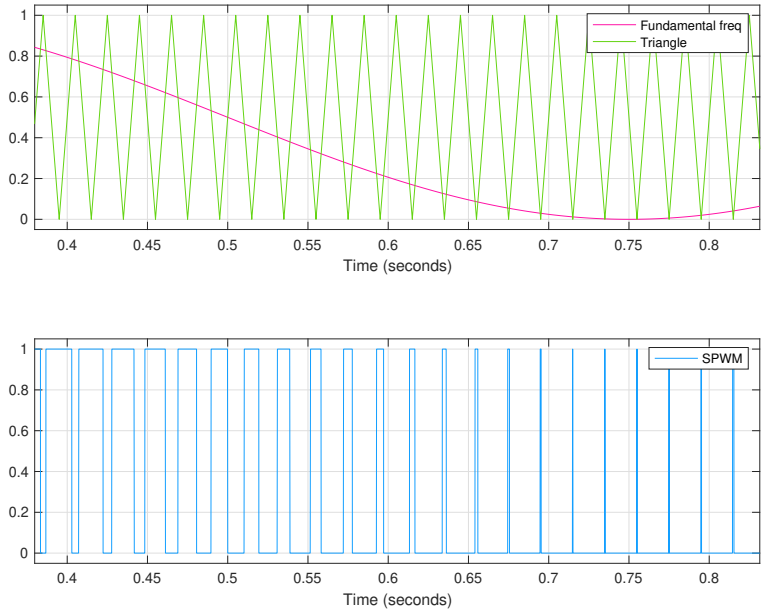

Figure 2.18: PWM slowly decreasing width of the pulse.

2.3.5.2 Space vector PWM

High side switches in 3 phase inverter shown in figure 2.5 have 2^3 combinations. Low side switches are complements of high side switches. All zeros and ones are invalid states so the rest of the combinations can be expressed as vectors in a hexagon vector space shown in figure 2.20 [25]. Vectors and switch combinations are listed in table 2.3. by modulating each nearby vectors' magnitude the average voltage U_{ref} can be rotated. For a rotating U_{ref} reference voltage is generated by injecting 3rd harmonic to a sinusoidal voltage shown in figure 2.21. Space vector PWM provides 15.4% higher [14] [26] DC voltage utilization compared to sinusoidal PWM. 3 phase reference voltage is shown in figure 2.22. Space vector PWM signal is generated from this reference signal the same way discussed in section 2.3.5.1 which is shown in figure 2.23.
Mathematical analysis and generation of Space vector PWM with a digital processor are quite complex and are beyond the discussion of this thesis. So they are not included here.

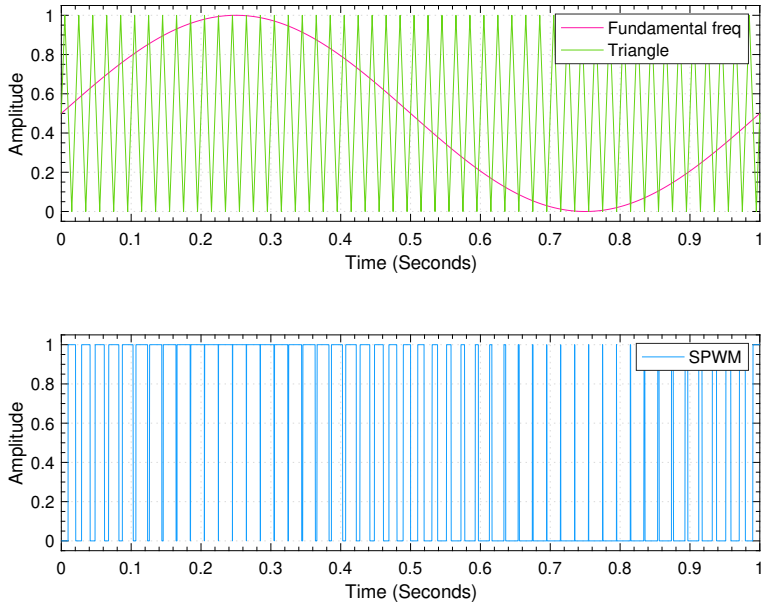

Figure 2.19: Sinusoidal PWM generation.

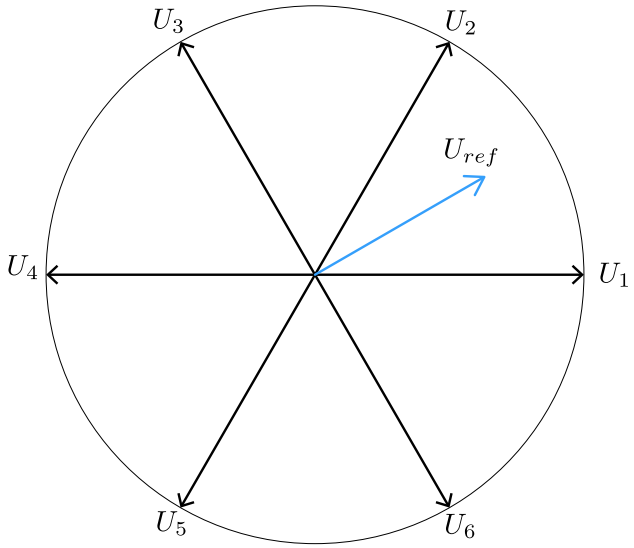

Figure 2.20: Space Vectors.

Space Vector	g1	g3	g5
U_1	1	0	0
U_2	1	1	0
U_3	0	1	0
U_4	0	1	1
U_5	0	0	1
U_6	1	0	1

Table 2.3: Space vectors with inverter gate signal.

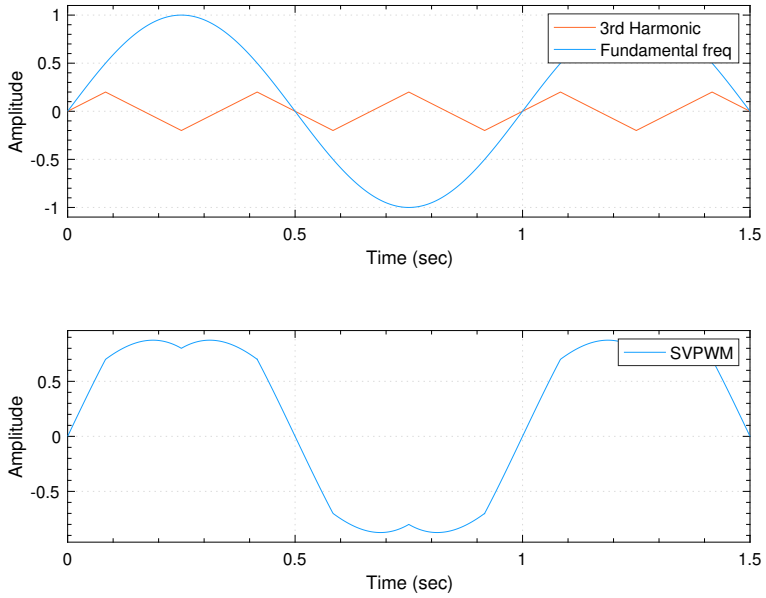

Figure 2.21: Adding 3rd harmonic to fundamental frequency.

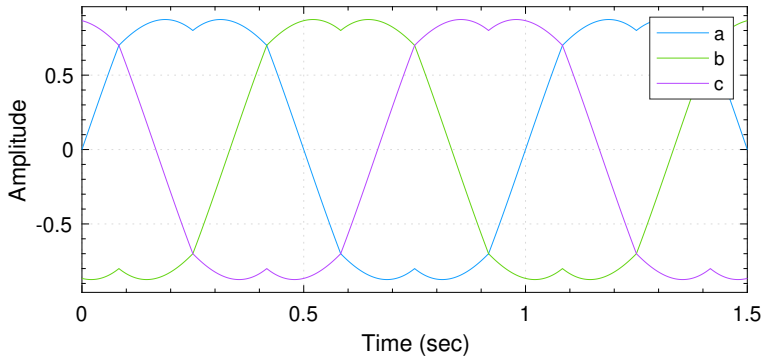

Figure 2.22: 3 phase space vector reference signal.

2.3.6 Startup issues with FOC and rotor alignment

Figure 2.13 and equations 2.17,2.19,2.23,2.24 show that there must be some speed to calculate angle, v_d and v_q. It is also true that the control system designed in this thesis has a minimum running speed, below which angle calculation will be inaccurate and the motor will stall. To avoid this start-up and minimum speed condition a few steps can be taken. one of them is to start the motor open-loop with a constant Vd and Vq. After minimum speed, the controller can slowly take over to avoid vibration. But this technique comes with problems too. Start-up condition must be tuned to known load. Any unknown load can cause rapid acceleration or stall.

This thesis deals with the start-up condition by changing the initial angle. At start-up, the FOC algorithm has no idea of the angle of the rotor. So a small voltage is provided to v_d, strengthening the magnetic field of the rotor causing the rotor to align with the known stator magnetic field. This also provides a small initial rotation, enough for the decoupling block to calculate v_d and v_q voltages which in turn provides the necessary voltage to the motor. Figure 2.24 shows the initial angle and RPM change during start-up.
At start-up, the control system performs the following actions,

Step 1: Disable current controllers
Step 2: Disable speed controller

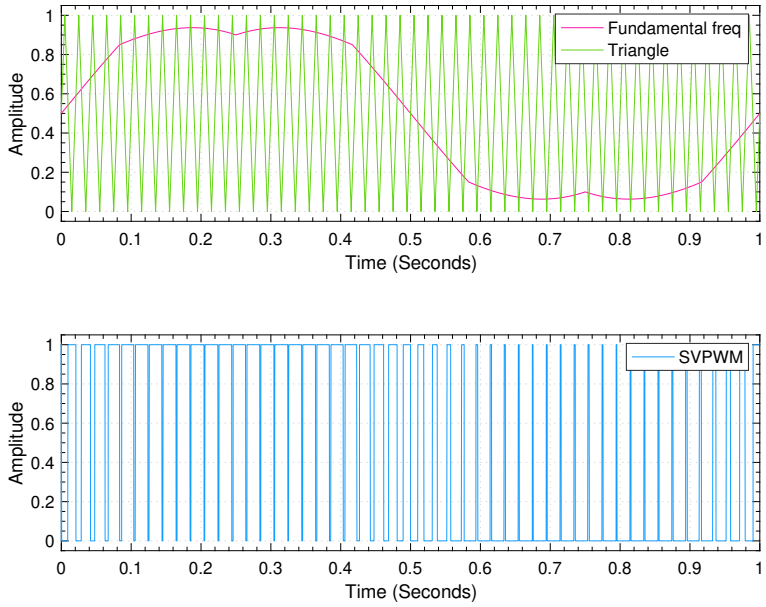

Figure 2.23: Space vector PWM generation.

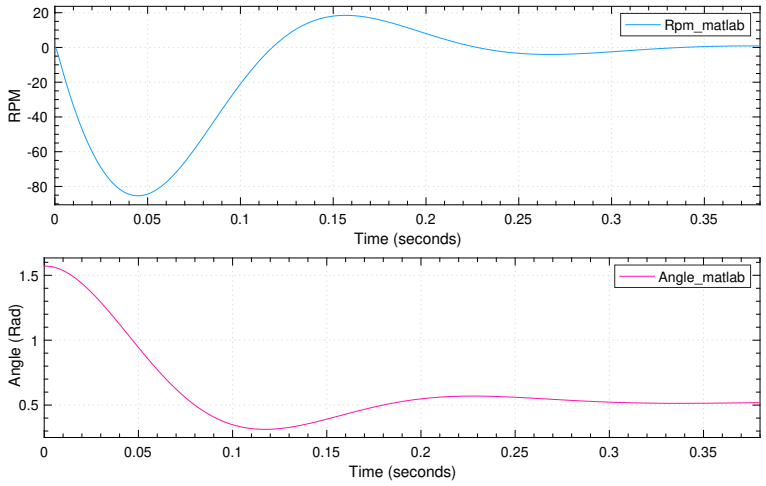

Figure 2.24: Rotor alignment during startup.

Step 3: Set initial angle to $\pi/6$
Step 4: Apply voltage to d-axis to align the rotor to predefined angle from step 3.
Step 5: Enable current and speed controllers.

2.4 PI controller tuning and motor parameter dependency

The gain of the PI controller is calculated based on motor parameters [27]. Proportional and integral gain is calculated from motor phase resistance, inductance, and rotor inertia. Gains can be found from

the following equations. Matlab script in appendix B shows the calculation used in simulation.

$$w_m = R_s/L_d \tag{2.31}$$
$$w_c = 5 * w_m \tag{2.32}$$
$$Ki_c = w_c^2 * L_d \tag{2.33}$$
$$Kp_c = w_c * L_d \tag{2.34}$$
$$w_s = w_c/10 \tag{2.35}$$
$$Ki_s = w_s^2 * J \tag{2.36}$$
$$Kp_s = w_s * J \tag{2.37}$$

So in the case of a new motor, these parameters need to be updated manually before running the motor. This process can be automated if motor parameter identification is included in the control system. Similar process is discussed in [28].

2.5 Battery low voltage and field weakening

Part of the goal of this thesis is to run a PMSM with a constant RPM without exceeding phase current limitation. Low battery voltage causes low inverter output voltages. Also, motor back EMF is directly proportional to rotor speed. From equation 2.19, higher back emf $\lambda\omega_e$, will reduce i_q current which in turn limits the rotor's maximum speed.

One of the methods to maintain high RPM is to weaken the magnetic field of the permanent magnets. d-axis current is aligned with rotor magnetic field which was discussed in 2.3. Permanent magnets have fairly constant magnetic flux [29]. Until now d-axis reference was set to zero to achieve maximum torque. But applying currents to the d-axis can weaken or strengthen the rotor magnetic field. Applying a negative current to the d axis will weaken the flux. There are other methods of field weakening control [30–34]. The equation 2.19 also shows that v_q is dominant at a high load, negative i_d allows lower v_q for the same rotor speed.

Setting negative i_d reference will allow the controller to apply appropriate voltage by the inverter. But too much negative current reference may exceed the current limits for the inverter or the motor.

CHAPTER 3

Simulation

3.1 Introduction

Computer simulation of any model is the ideal way of understanding the behavior and overall performance. Deploying and running a new control algorithm of a motor to an existing system can be dangerous in real life.

To avoid damage to the motor or any other component both Six step control and Field oriented control were simulated in Simulink. The simulation contains a PMSM motor model, that has parameters specified in table A.1.

Different parameter values were tested by applying different conditions and some of the values were tweaked to achieve maximum performance. The control system was designed using the Linix motor [35], provided by NXP and then tested on Boel motor [14] to check the performance and verify questions asked in Chapter 1.

3.2 Simulation Overview

The Simulink model of FOC control is shown in figure 3.1. The model was designed to be implemented in an embedded system. So control system and input-output were kept separated to make it easier for hardware implementation.

FOC controller block consists of the control algorithm, shown in figure 3.2. Hall decoder reads hall signals and performs calculations to provide angle and speed measurement discussed in section 2.3.4. Decoupling block executes equations mentioned in section 2.3.3 and outputs calculated v_d and v_q. A detailed view of this block is shown in figure 3.5.

The speed control block compares the current speed and measured speed from the Hall decoder block and produces the reference q-axis current for the input speed. Detailed views are shown in figure 3.7. Current measurement block measures phase currents using ADC then performs Clarke and Park transform to produce d and q axis currents shown in figure 3.3. The difference between speed control blocks output and Current measurement blocks output is the d and q axis error signals.

The current controller takes these error signals as input and PI controllers output d and q axis voltage based on Kp and Ki gains calculated from motor variables. These outputs are then added with decoupling blocks output to produce d and q axis voltage by the Inverter to generate space vectors and space

vector PWM.The inverter control block, detailed view in figure 3.4, shows the generation of space vector by the inverse Park and Clarke transform to produce U_{ref} from d and q axis voltage discussed as in section 2.3.5.2.

Rotor align block performs initial rotor alignment discussed in section 2.3.6 to align rotor to a predefined angle by applying a voltage at d axis shown in the figure. Initialization block provides a signal to sync this initialization and disable all other blocks as necessary.

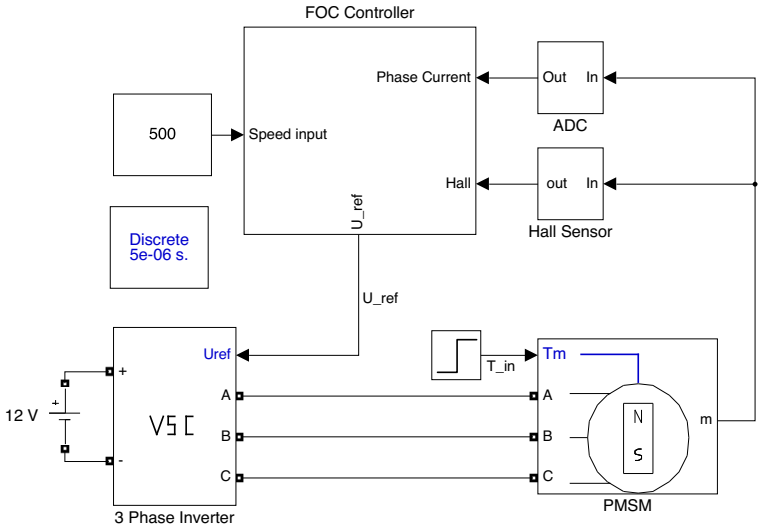

Figure 3.1: Field oriented control Simulink model.

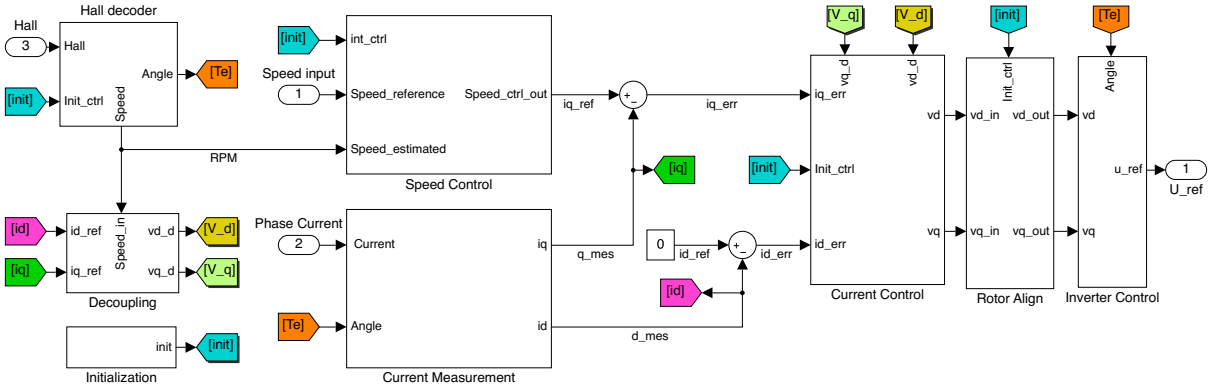

Figure 3.2: FOC controller

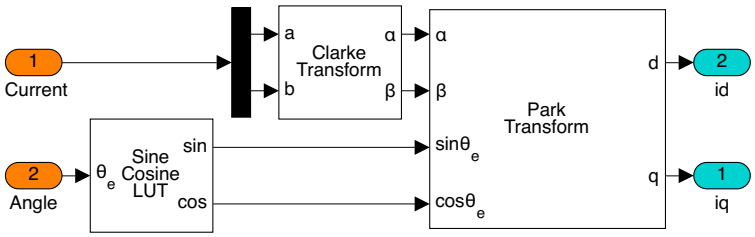

Figure 3.3: Current measurement

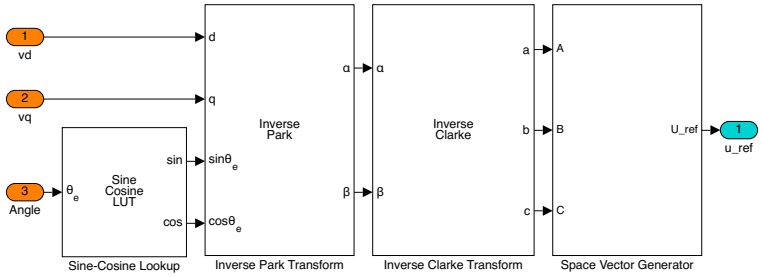

Figure 3.4: Inverter control block.

$$\frac{di_d}{dt} = \frac{v_d}{L_d} - \frac{R_s\ i_d}{L_d} + \frac{L_q}{L_d}.\omega_e.i_q$$

$$v_d = R_s i_d + L_d \frac{di_d}{dt} - \omega_e.L_q.i_q$$

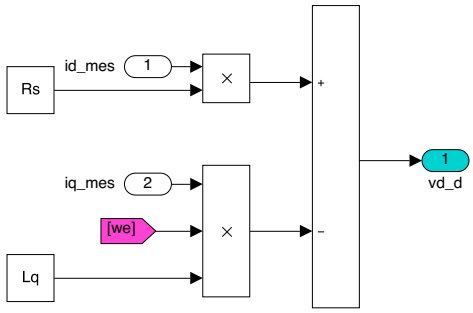

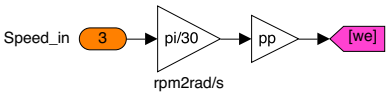

$$\frac{di_q}{dt} = \frac{v_q}{L_q} - \frac{R_s.i_q}{L_q} - \frac{L_d}{L_q}.\omega_e.i_d - \lambda\frac{\omega_e}{L_q}$$

$$v_q = R_s i_q + L_q \frac{di_q}{dt} + \omega_e.L_d.i_d + \lambda\omega_e$$

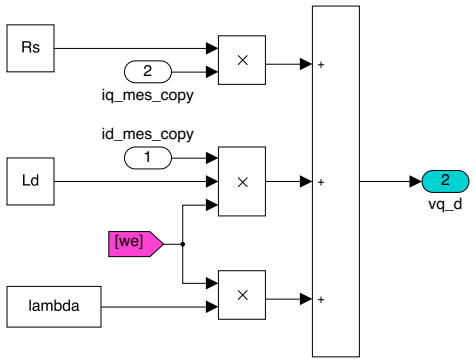

Figure 3.5: Decoupling.

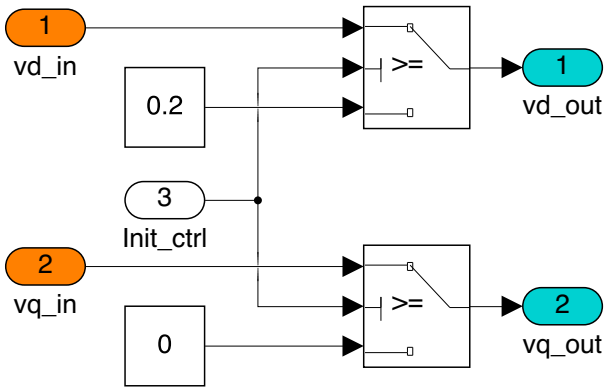

Figure 3.6: Initial rotor alignment.

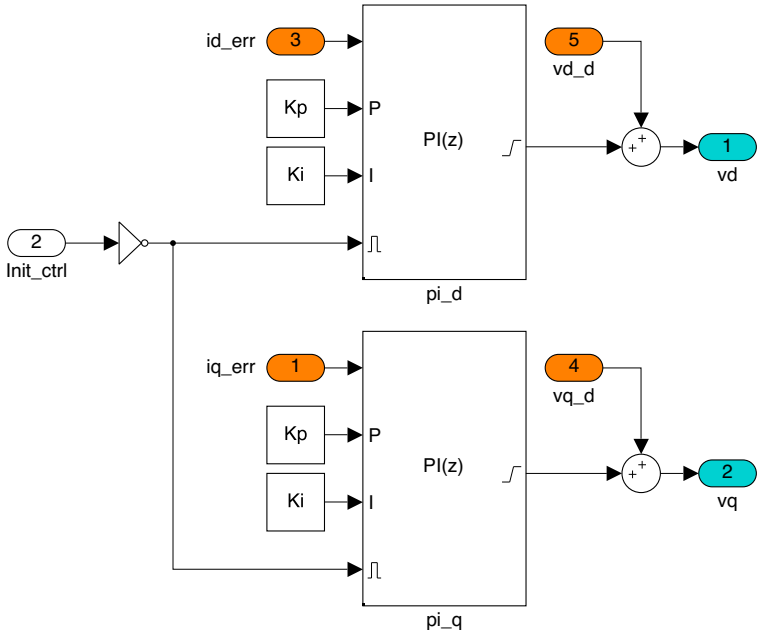

Figure 3.7: Current controllers.

3.3 Speed and current controller

There are two feedback loops to control a PMSM motor in this algorithm. Speed control loop and current control loop. This is also described in 2.3.2. Current controllers' gain is chosen to be much faster than the speed controller to maintain stability.

Speed controller receives speed feedback from hall sensor decoder and outputs necessary voltage command for Current controllers. The current controllers constantly monitor motor phase currents and based on the speed controller's output, provide voltage command to the Space vector modulator. The decoupling block's output is added with the current controller's output to control d and q axis voltage independently.

3.3.1 Speed control

Speed controller amplifies the error signal produced by the controller from the difference between user input and current estimated speed input. Speed controllers gain is calculated from motor specifications shown in the script B. On the figure 3.9 it is shown that the speed controller is tracking input speed with no load condition. Figure 3.10 shows the same motor running at 500 RPM while torque on 0.02 Nm applied at 1.5 sec.

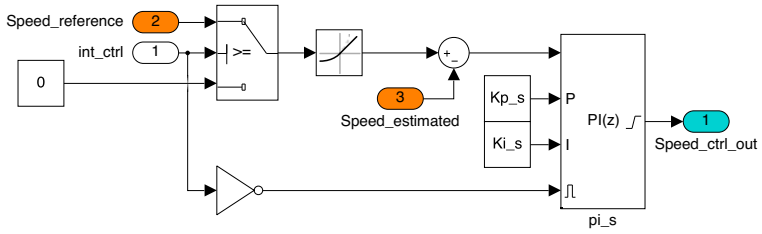

Figure 3.8: Speed controller.

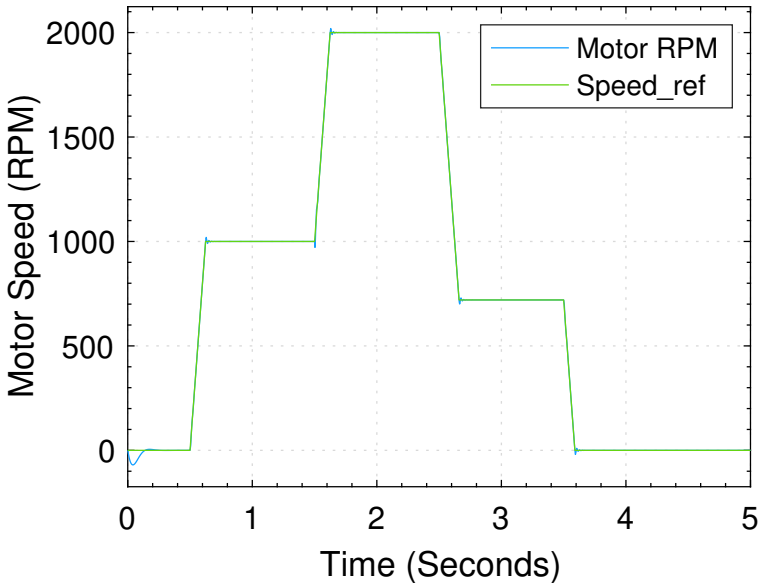

Figure 3.9: Speed tracking by the controller without load.

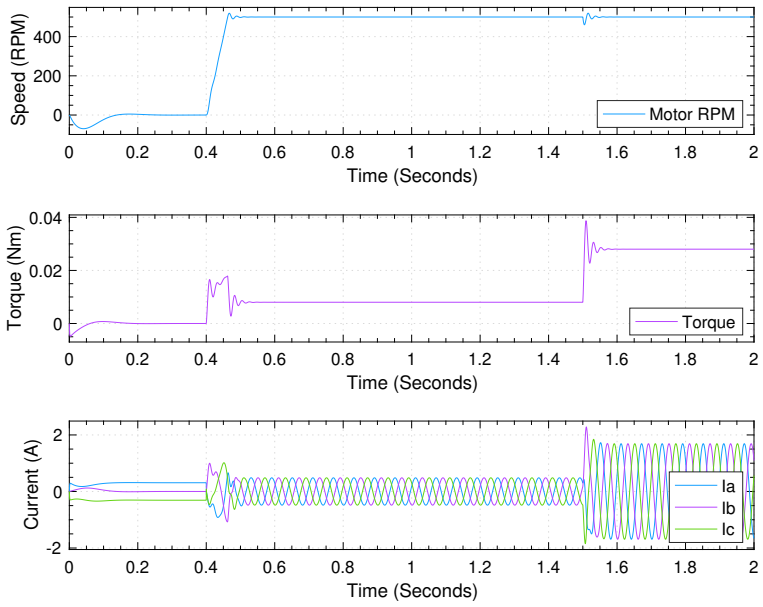

Figure 3.10: Fixed RPM with 0.02 Nm external load.

3.3.2 Current control

Figure 3.13 shows the transformation results of phase currents. d and q axis currents are transformed using Clarke and park transformation. Figure 3.14 shows the output v_d and v_q which is calculated from decoupling block and current measurement block. Inverter control block produces necessary space vector signal as output is shown in figure 3.15. Figure 3.16 shows phase currents for the same time.

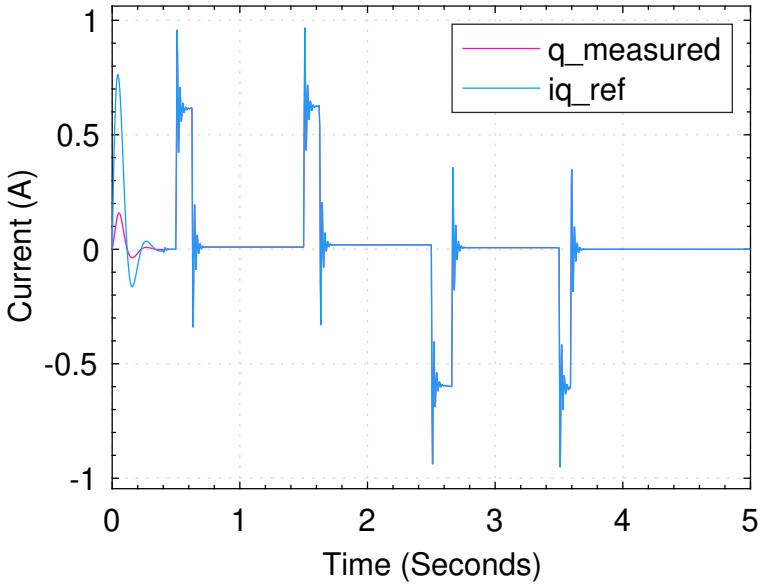

Figure 3.11: q-axis current control

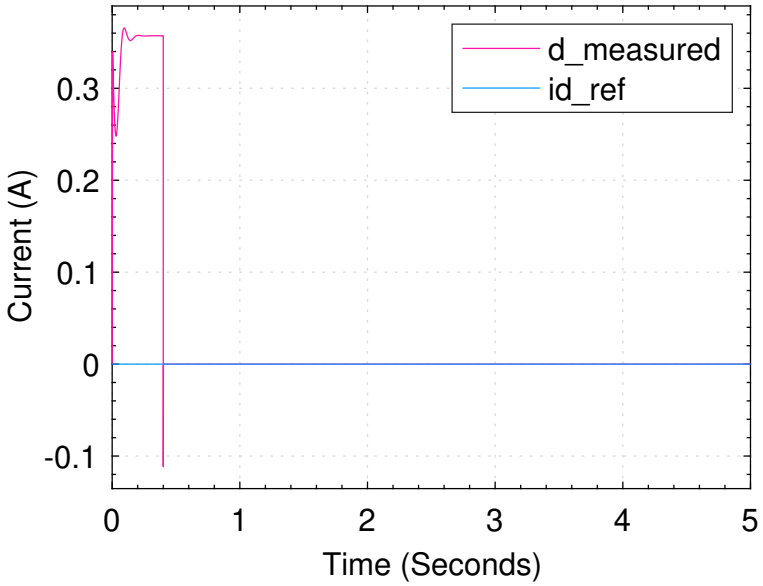

Figure 3.12: d-axis current control

Figure 3.11 and 3.12 shows current tracking for the same simulation on figure 3.9. Differences at the beginning of the simulation is from rotor alignment. After initial rotor alignment id_{ref} is zero. Measured d-axis current also measures the same value. Changes in speed reference require higher or lower i_q current. Figure 3.11 and 3.12 shows reference currents are well tracked by the current controllers.

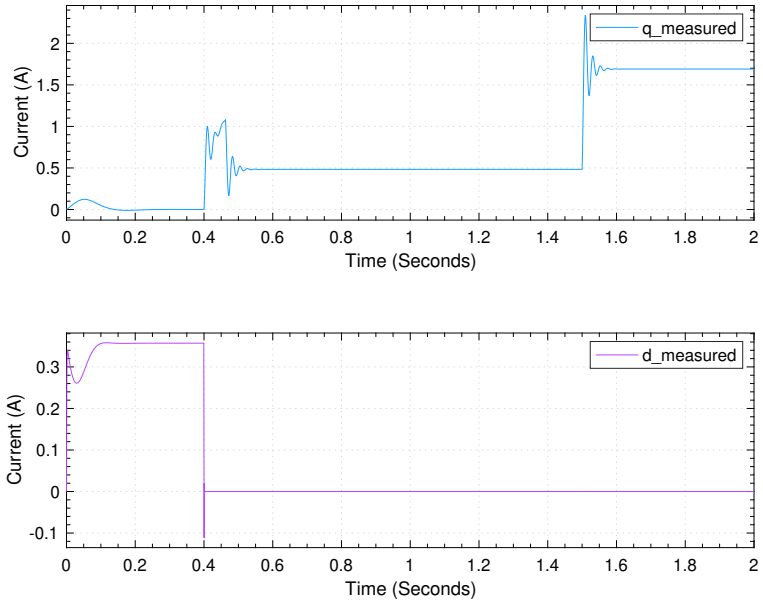

Figure 3.13: Measured currents

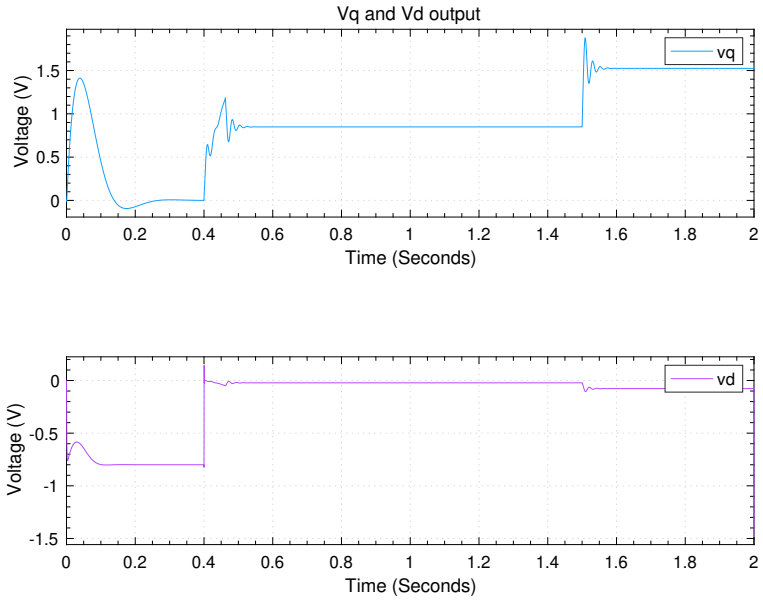

Figure 3.14: Vd and Vq voltage outputs.

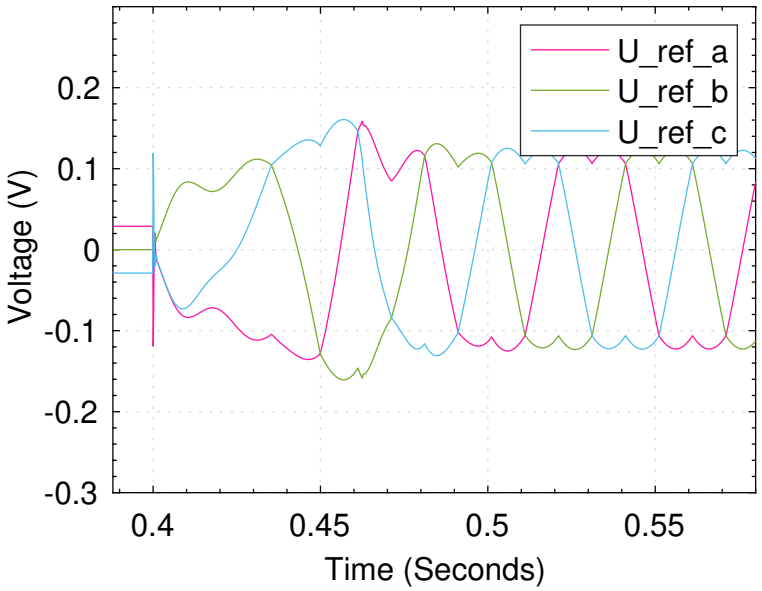

Figure 3.15: Space vector generation.

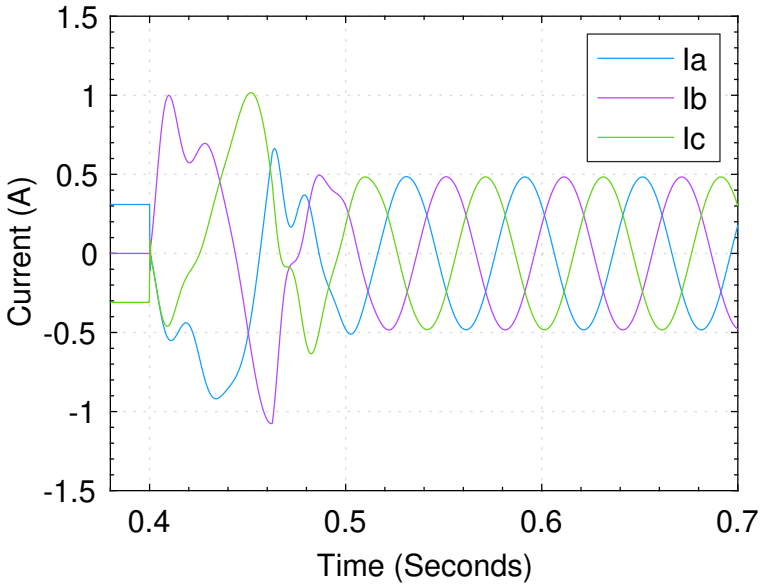

Figure 3.16: Phase currents

Figure 3.10 also shows that the current controllers control phase currents according to the load or input speed. When a torque was applied externally at 1.5 sec, more current was applied to the motor to sustain 500 RPM by the controller. Figure 3.14 also shows higher v_q voltage.

3.4 Speed and Angle simulation

3.4.1 Speed estimation using hall sensors

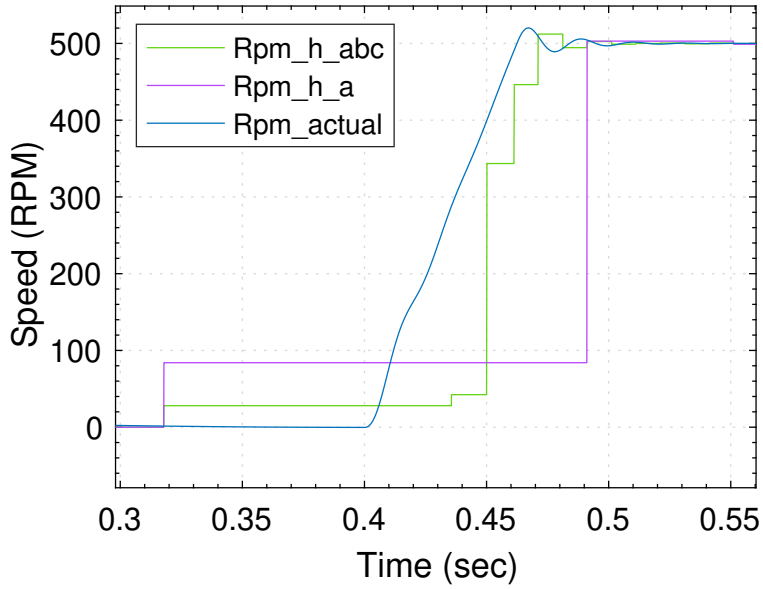

Figure 3.17: RPM calculation using 1 and 3 hall sensors and actual RPM.

Figure 3.17 shows speed calculation results from one hall sensor and 3 hall sensors. Using 3 hall sensors provides better speed resolution as mentioned in section 2.3.4.1.

3.4.2 Angle estimation simulation

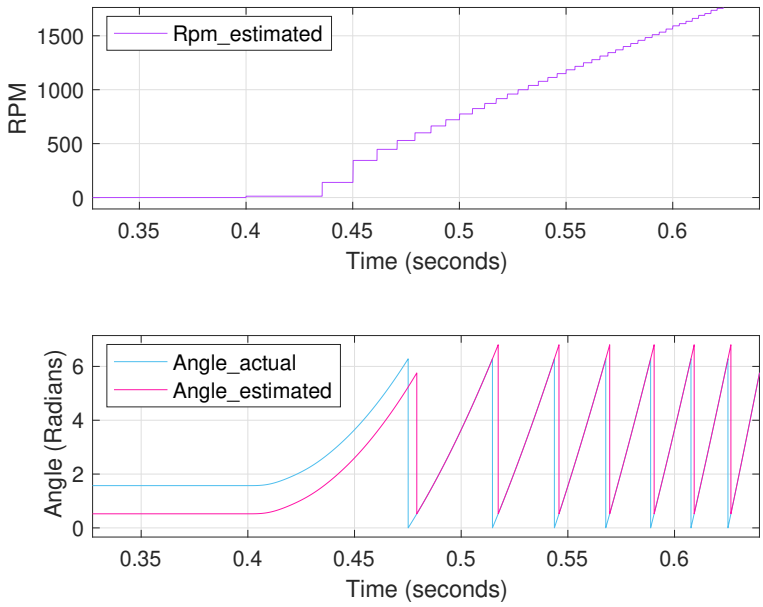

Figure 3.18: Estimated angle from calculated speed.

Figure 3.18 shows that as soon as the motor speeds up, the estimated gets closer to the actual angle. So at higher speeds, the estimation error will be almost zero.

3.5 Low battery voltage operation

Section 2.5 discusses techniques to maintain high RPM at lower battery voltage. To simulate low voltage operation the motor was run at various DC voltage levels simulating different battery charge levels. Measured parameters are listed in table 3.1.

DC voltage is measured from the battery terminal. id_ref is the applied id reference for different cases. id and iq are dq currents, measured at output Current measurement block shown in figure 3.3. vd and vq are the controller output voltage to the inverter, measured at the current controllers' output, shown in figure 3.7. For motor phase currents, only phase A current is shown in the table as the rest of the phases are the same. The mod index is the modulation index calculated by the following equation,

$$m_a = \frac{\sqrt{v_d^2 + v_q^2}}{\frac{DC}{2}} \tag{3.1}$$

			Measured(A)		Output(V)		Current(A)	Mod index
DC(V)	id_ref(A)	RPM(max)	id	iq	vd	vq	Phase a	m_a
250	0	3546	0	2.8	-2	146	2.8	1.17
	-2	3719	-2	3	-2.5	147	3.8	1.18
	-4	3866	-4	3.2	-2.6	146	5.1	1.17
	-6	4117	-6	3.4	-3	146	6.9	1.17
	-8	4218	-8	3.7	-3.4	145	8.8	1.16
	-10	4435	-10	4	-3.9	145	10.8	1.16
225	0	3196	0	2.5	-1.6	132	2.6	1.17
	-2	3328	-2	2.6	-1.9	131	3.5	1.16
	-4	3474	-4	2.9	-2.1	131	4.9	1.16
	-6	3630	-6	3.1	-2.5	131	6.7	1.16
	-8	3806	-8	3.3	-2.8	131	8.6	1.16
	-10	3992	-10	3.6	-3.2	131	10.6	1.16
200	0	2843	0	2.3	-1.4	117	2.3	1.17
	-2	2960	-2	2.6	-1.6	117	3.3	1.17
	-4	3090	-4	2.6	-1.6	117	4.8	1.17
	-6	3231	-6	2.8	-2	117	6.6	1.17
	-8	3426	-8	3	-2.3	119	8.5	1.19
	-10	3609	-10	2.4	-2.7	119	10.4	1.19
180	0	2565	0	2.1	-1.2	106	2.1	1.18
	-2	2678	-2	2.2	-1.3	106	3.2	1.18
	-4	2803	-4	2.3	-1.5	106	4.7	1.18
	-6	2920	-6	2.5	-1.6	106	6.5	1.18
	-8	3086	-8	2.7	-1.8	106	8.4	1.18
	-12	3374	-12	3.2	-2.4	105	12.4	1.17
	-15	3657	-15	3.6	-3	104	15.4	1.16

Table 3.1: Low battery voltage simulation result.

The table shows that applied negative d-axis current increases RPM. This can be used partly to alleviate speed loss during low battery voltage. id_{ref} can be reduced as long as phase currents do not exceed the hardware limit. Here rated maximum phase current is 100 A.
The first case can be considered where without any field weakening the motor produces 3500 RPM at 250V. This speed was maintained throughout the voltage drop cases. Even at 180 V, the motor can produce 3500 RPM with a higher phase current. The calculated modulation index also shows 15% overmodulation with slight roundoff errors. This is true for the space vector modulation technique.

3.6 Running different motor

The Boel motor in appendix A.1 was run with 200 VDC, without making any change in the control system. Figure 3.19 shows speed control performance and figure 3.20 shows the output motor torque.

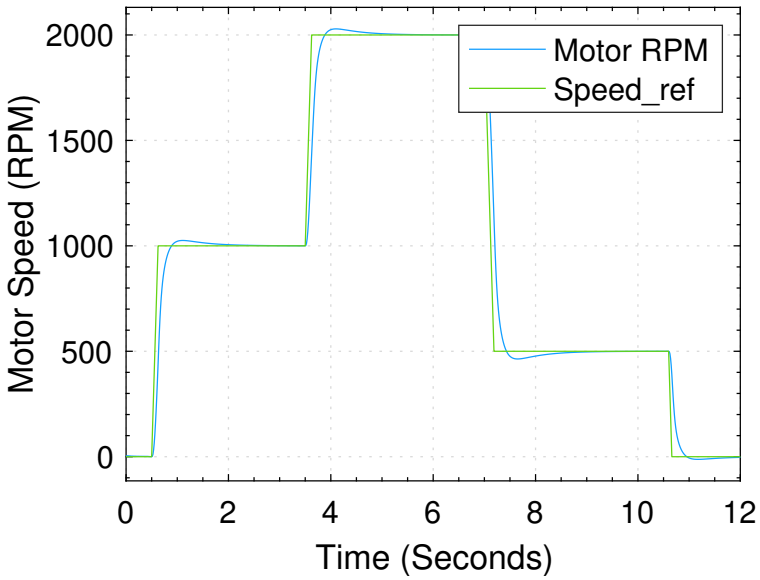

Figure 3.19: Boel motor speed control.

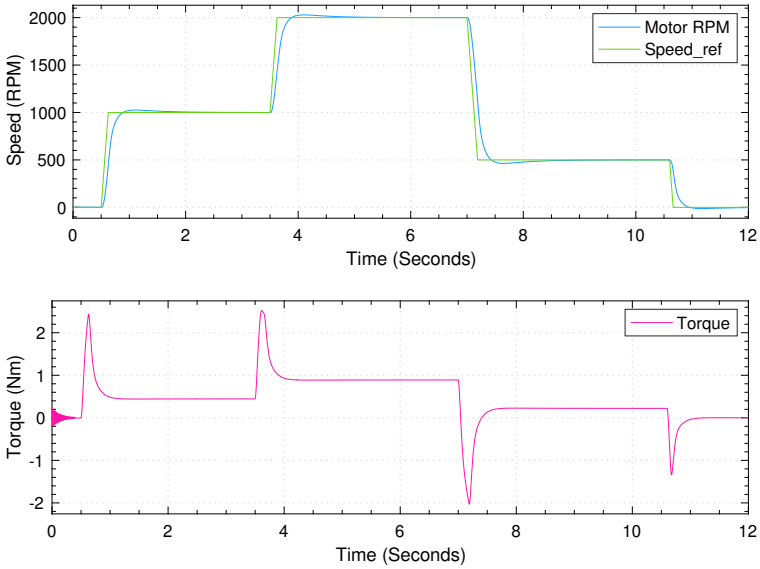

Figure 3.20: Motor speed and output torque of the Boel motor.

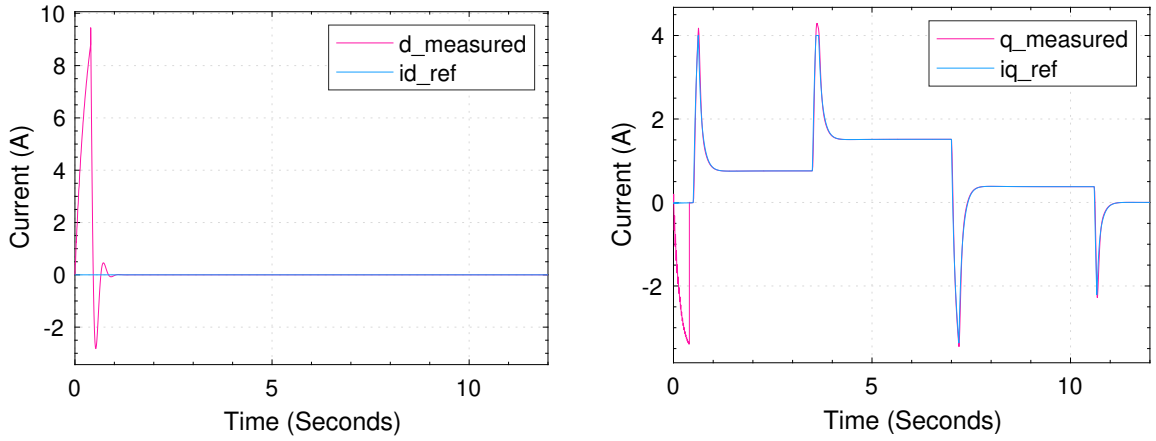

(a) d-axis current control.

(b) q-axis current control.

Figure 3.21: Current control performance of the Boel motor.

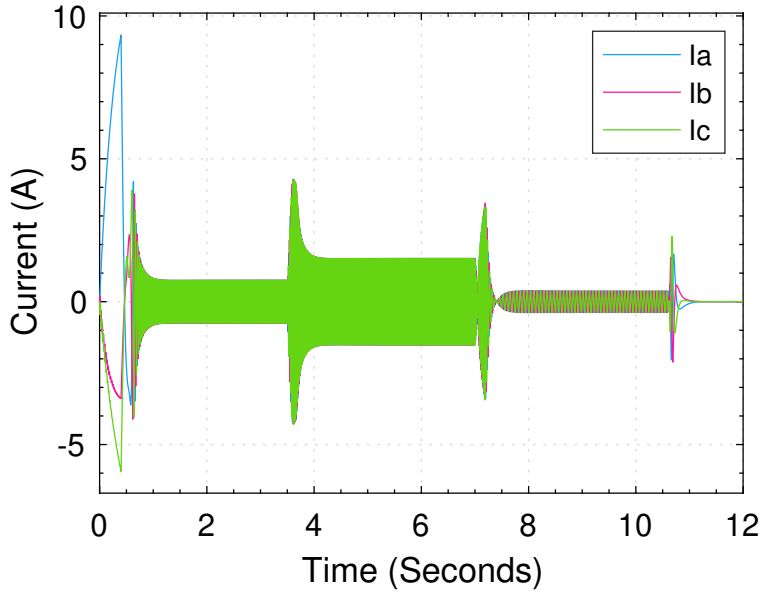

Figure 3.22: Phase currents for the given reference speed.

Figure 3.22 shows phase currents at no load operation for the given speed reference. Figure 3.21b and 3.21a shows current control performance with new control gains. This proves that it is possible to run a separate motor with this control system with new current and speed control gains as long as the motor specifications are known.

CHAPTER 4

Discussion

4.1 Introduction

This chapter contains a discussion between the questions asked in chapter 1 theories provided in chapter 2 and results from the simulation chapter.

4.2 Results

The primary goal of this thesis was to run a PMSM and investigate the situation for low battery voltage and maintain RPM and run a different motor with minimum or no change in the control algorithm.

Speed tracking simulations in Figures 3.9, 3.10, 3.19 and 3.20 show that the control system can run a PMSM with minimum overshoot while input speed reference changes. Speed control is stable and fast. As the speed is estimated from the hall sensors speed calculation error minimizes with higher speed. Angel estimation error is multiplied by the speed estimation. So minimum speed error means low angle estimation error.

Table 3.1 shows the performance during low battery voltage operation. RPM values at lower id_{ref} show that it is possible to maintain a high RPM at low battery voltage. The theory section 2.5 discussed that field weakening will allow higher motor speed at lower dc voltage levels with higher phase current. But this high speed comes at the cost of torque. Since the battery has less power at lower voltages, the motor can not produce the same power, in other words, maintain high speed and high torque at the same time. So when battery voltage drops controller applies low id_{ref} to increase the speed at lower torque output. This can be observed at phase current too. With lower id_{ref}, phase current increases to maintain higher speeds. Also in section 2.3.5.2, it was mentioned that Space vector modulation allows 15% more use of DC voltage. Maximum speed is achieved when the motor is run at maximum DC voltage. So in the case of space vector modulation, if modulation index $m_a = 1.15$ then the motor will run at maximum speed. Modulation index results and RPM values in the table prove this. There are some roundoff errors, which caused $m_a > 1.15$.

For the second motor, only gains of current and speed controller were changed. So the second question asked in chapter 1 is yes, the control system can run any motor as long as the specifications are known and have fixed d and q axis inductances.

4.3 Methods

Field-oriented control is not a new control algorithm and all the IEEE papers and books used in this thesis work show the same equations for implementation. But improvement the possibilities of the algorithm are endless. Few estimation techniques were used in this thesis work with better estimation the control algorithm will perform better and become robust. In [24] speed estimation was done by using one hall sensor but in this thesis use if three hall sensor technique shows better performance.

Currently, negative speed is not taken into account. So the motor can only run in one direction. Direction identification requires detecting predefined hall patterns, which is kept as future work.

There are motors available that have variable d and q axis inductances. This control system can not run these types of motors yet. Future improvements are necessary to run these motors.

Hardware implementation raises safety concerns. At the time of implementation in an embedded system, the control system might need modification or tweaking based on performance. So this model despite having good simulation performance is not yet ready to be implemented in hardware.

CHAPTER 5

Conclusion

5.1 Conclusion

The thesis intended to implement closed-loop field-oriented control with hall sensor feedback for speed and angle estimation and study the case for low battery voltage and the use of different motors. The theory chapter provides theories and mathematical analysis for the control algorithm. The simulation results show that positive outcomes for the research questions asked in chapter one.

5.2 Future works

This project already shows good performance in simulation. However, lot of improvements can still be done. A few of them are,

- Implementation of negative speed.
- making the control algorithm sensorless.
- Making the estimators robust to handle low speeds
- Improving the control algorithm to run motors that have d and q axis inductance matrix.
- Making the control system automatic. So that it can measure motor variables by running a self-test algorithm.

References

[1] C.-I. Nicola, M. Nicola, A. Vintilă, and D. Sacerdoţianu, "Identification and sensorless control of pmsm using foc strategy and implementation in embedded system," in *2019 International Conference on Electromechanical and Energy Systems (SIELMEN)*, pp. 1–6, 2019.

[2] L. Qu, L. Qu, and W. Qiao, "A linear active disturbance rejection controller-based sensorless control scheme for pmsm drives," in *2019 IEEE Energy Conversion Congress and Exposition (ECCE)*, pp. 792–797, 2019.

[3] L. Yu, C. Wang, H. Shi, R. Xin, and L. Wang, "Simulation of pmsm field-oriented control based on svpwm," in *2017 29th Chinese Control And Decision Conference (CCDC)*, pp. 7407–7411, 2017.

[4] F. Jin, W. Qian, H. Bai, D. Lu, and B. Cheng, "Using one fpga to control two high-switching-frequency pmsm drive systems through a novel time-division multiplexing method," in *2018 IEEE Applied Power Electronics Conference and Exposition (APEC)*, pp. 998–1002, 2018.

[5] M. Caruso, A. Di Tommaso, R. Miceli, C. Nevoloso, G. Vassallo, and G. Vitamia, "Foc with resolver implementation for pmsm drives by using a low cost atmel sam3x8e microcontroller," in *2020 Fifteenth International Conference on Ecological Vehicles and Renewable Energies (EVER)*, pp. 1–8, 2020.

[6] A. O. di Tommaso, R. Miceli, G. R. Galluzzo, and M. Trapanese, "Efficiency control for permanent magnet synchronous generators," in *2006 IEEE International Conference on Industrial Technology*, pp. 2079–2084, 2006.

[7] M. Caruso, A. O. Di Tommaso, M. Lombardo, R. Miceli, C. Nevoloso, and C. Spataro, "Experimental comparison of two control algorithms for low-saliency ratio interior permanent magnet synchronous motors," in *2018 Thirteenth International Conference on Ecological Vehicles and Renewable Energies (EVER)*, pp. 1–6, 2018.

[8] M. Caruso, A. O. Di Tommaso, R. Miceli, C. Nevoloso, C. Spataro, and F. Viola, "Enhanced loss model algorithm for interior permanent magnet synchronous machines," in *2017 AEIT International Annual Conference*, pp. 1–6, 2017.

[9] M. Caruso, A. O. Di Tommaso, F. Genduso, and R. Miceli, "Experimental investigation on high efficiency real-time control algorithms for ipmsms," in *2014 International Conference on Renewable Energy Research and Application (ICRERA)*, pp. 974–979, 2014.

[10] C. Cavallaro, A. Di Tommaso, R. Miceli, A. Raciti, G. Ricco Galluzzo, and M. Trapanese, "Analysis a dsp implementation and experimental validation of a loss minimization algorithm applied to permanent magnet synchronous motor drives," in *IECON'03. 29th Annual Conference of the IEEE Industrial Electronics Society (IEEE Cat. No.03CH37468)*, vol. 1, pp. 312–317 vol.1, 2003.

[11] G. Schettino, C. Buccella, M. Caruso, C. Cecati, V. Castiglia, R. Miceli, and F. Viola, "Overview and experimental analysis of mc spwm techniques for single-phase five level cascaded h-bridge fpga controller-based," in *IECON 2016 - 42nd Annual Conference of the IEEE Industrial Electronics Society*, pp. 4529–4534, 2016.

[12] M.-F. Tsai and H.-C. Chen, "Design and implementation of a cpld-based svpwm asic for variable-speed control of ac motor drives," in *4th IEEE International Conference on Power Electronics and Drive Systems. IEEE PEDS 2001 - Indonesia. Proceedings (Cat. No.01TH8594)*, vol. 1, pp. 322–328 vol.1, 2001.

[13] M. T. Kassa and D. Changqing, "Design optimazation and simulation of pmsm based on maxwell and twinbuilder for evs," in *2021 8th International Conference on Electrical and Electronics Engineering (ICEEE)*, pp. 99–103, 2021.

[14] A. Kronberg, "Salient pole motor inverter design: with implementation of space vector modulation," 2012.

[15] M. Johansson, "Evaluation of sensor solutions & motor speed control methods for bldcm/pmsm in aerospace applications," 2017.

[16] X. Gao, "Bldc motor control with hall sensors based on frdm-ke02z," 2013.

[17] D. Daniel, "Pmsm and foc theory." https://community.nxp.com/t5/NXP-Model-Based-Design-Tools/Module-2-PMSM-and-FOC-Theory/m-p/761926.

[18] G. Alain and J. De Leon-Morales, *Sensorless AC Motor Control: Robust Advanced Design Techniques and Applications*. SPRINGER, May 2005.

[19] Fadili, Abdelmounime El Magri, Fouad Giri, and Abderrahim El , *Control Models for Synchronous Machines*, ch. 3, pp. 41–56. John Wiley & Sons, Ltd, 2013.

[20] Wikipedia contributors, "Alpha–beta transformation — Wikipedia, the free encyclopedia," 2021. [Online; accessed 14-March-2021].

[21] I. WESTIN, "Sensorless control of a pmsm," 2016.

[22] Mathworks, "Permanent magnet synchronous machine." https://se.mathworks.com/help/physmod/sps/powersys/ref/permanentmagnetsynchronousmachine.html.

[23] F. Semiconductor, "Sensorless pmsm vector control with a sliding mode observer for compressors using mc56f8013," 2008.

[24] D. Daniel, "Motor control class: Lecture 10 - speed estimator." https://community.nxp.com/t5/NXP-Model-Based-Design-Tools/Motor-Control-Class-Lecture-10-Speed-Estimator/m-p/681518.

[25] Mathworks, "Space vector modulation (svm) for motor control." https://se.mathworks.com/solutions/power-electronics-control/space-vector-modulation.html.

[26] L. Zhen, "Sinusoidal control of bldcm with hall sensors based on frdm-ke04z and tower board," 2014.

[27] L. Harnefors and H. Nee, "Control of variable speed drives applied signal processing and control," *Mälardalen University, Västeras, Sweden*, 2002.

[28] Mathworks, "Estimate pmsm parameters using recommended hardware." https://se.mathworks.com/help/mcb/gs/estimate-pmsm-parameters-using-recommended-hardware.html.

[29] T. Deng, Z. Su, J. Li, P. Tang, X. Chen, and P. Liu, "Advanced angle field weakening control strategy of permanent magnet synchronous motor," *IEEE Transactions on Vehicular Technology*, vol. 68, no. 4, pp. 3424–3435, 2019.

[30] R. U. Lenke, R. W. De Doncker, M.-S. Kwak, T.-S. Kwon, and S.-K. Sul, "Field weakening control of interior permanent magnet machine using improved current interpolation technique," in *2006 37th IEEE Power Electronics Specialists Conference*, pp. 1–5, 2006.

[31] D. Stojan, D. Drevensek, Z. Plantic, B. Grcar, and G. Stumberger, "Novel field-weakening control scheme for permanent-magnet synchronous machines based on voltage angle control," *IEEE Transactions on Industry Applications*, vol. 48, no. 6, pp. 2390–2401, 2012.

[32] Z. Lei, W. Xuhui, Z. Feng, K. Liang, and Z. Baocang, "Deep field-weakening control of pmsms for both motion and generation operation," in *2011 International Conference on Electrical Machines and Systems*, pp. 1–5, 2011.

[33] C.-T. Pan and J.-H. Liaw, "A robust field-weakening control strategy for surface-mounted permanent-magnet motor drives," *IEEE Transactions on Energy Conversion*, vol. 20, no. 4, pp. 701–709, 2005.

[34] L. Harnefors, K. Pietilainen, and L. Gertmar, "Torque-maximizing field-weakening control: design, analysis, and parameter selection," *IEEE Transactions on Industrial Electronics*, vol. 48, no. 1, pp. 161–168, 2001.

[35] F. Semiconductor, "Bldc sensorless reference design using mc56f8006," 2009.

APPENDIX A

Motor Specifications

In this project, Linix 45ZWN24-40 [35] and Boel motor [14] were simulated.

Parameter	Linix 45ZWN24-40	Boel Motor	Unit
Pole-pair number	2	2	$\sim$
Stator resistance	0.56	0.015	Ohm
Direct axis inductance	0.000375	0.004	H
Quadrature axis inductance	0.000435	0.001	H
Back-EMF constant	0.0135281	$\sim$	V*Sec/rad
Drive inertia	0.000012	0.003334	Kg*m^2
Maximum current	2.3	100	A
Rated speed	2000	3000	RPM
Friction	0.0001529694	0.00425	Nms

Table A.1: Motor specifications.

APPENDIX B

Matlab Script for PI gain calculation

```
clc
clear

% Motor Parameters for Linix / NXP motor

    pp = 2;                          % Pole pair
    Rs = 0.56;                       % Stator resistance [Ohm]
    Ld = 0.000375;                   % Direct axis inductance [H]
    Lq = 0.000435;                   % Quadrature axis inductance [H]
    Ke = 0.0135281;                  % Back-EMF constant [V.Sec/rad]
    J = 0.12e-4;                     % Drive inertia[kg.m2]
    lambda = sqrt(2/3) * Ke / pp;    % Flux linkage

% PI gain Calculation
    wm = Rs/Ld;
    wc = 5*wm;
    ws = wc / 10;

% Speed controller gain
    Ki_s = ws^2 * J;                 % Integral gain
    Kp_s = ws * J;                   % Proportional gain

% Current controller gain
    Ki = wc^2 * Ld;
    Kp = wc * Ld;

% Simulation Parameters
    Ts = 5e-6;                       % Sample time

% Speed calculation
    int_b = 0.01e-3;                 % Interrupt Base

disp('Motor parameters initialized!')
```